data shown in Figures 5.2 to 5.5 and 5.10 to 5.17 were extrapolated to the nodes of the relevant grid providing the nodal displacement values (u_n and v_n) for each node of the grid (see Figure D.2). Drawings at a scale of 4.5x life size were prepared for this purpose. Both the sand grain displacement contour diagrams as well as the rectangular grids, were drawn such that the pile shoe was located in the position it had attained at the end of any particular movement increment. Thus the u_n and v_n displacement components determined for each node represented the nodal movements required to generate the rectangular grids as drawn. Consequently, the node co-ordinates (x_n, y_n) required for substitution into the co-ordinate matrix were determined by subtracting the measured displacements from the known co-ordinates of the regular grid (see Figure D.2).

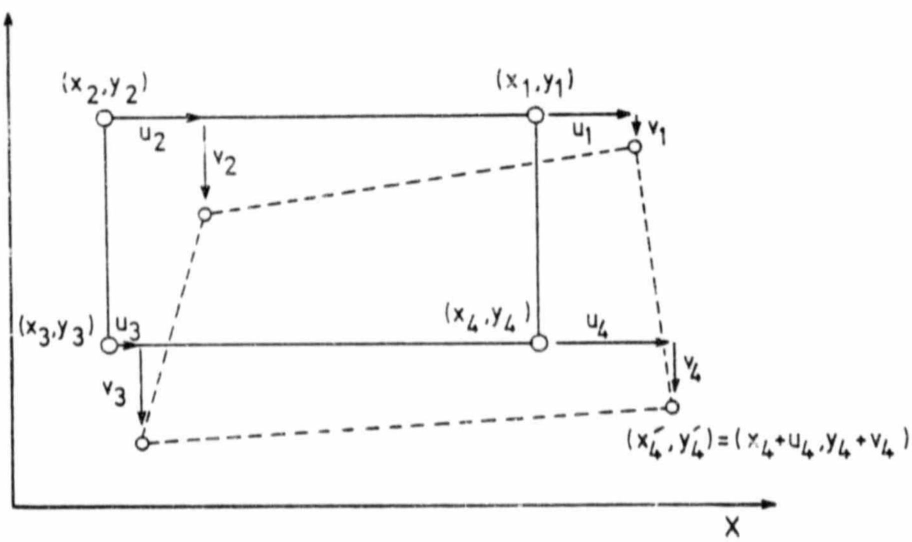

Figure D.1

Notation for deformation of a rectangular element

(x_n, y_n) = co-ordinates of undeformed element nodes.

u_n, v_n = displacements of nodes in X and Y directions respectively

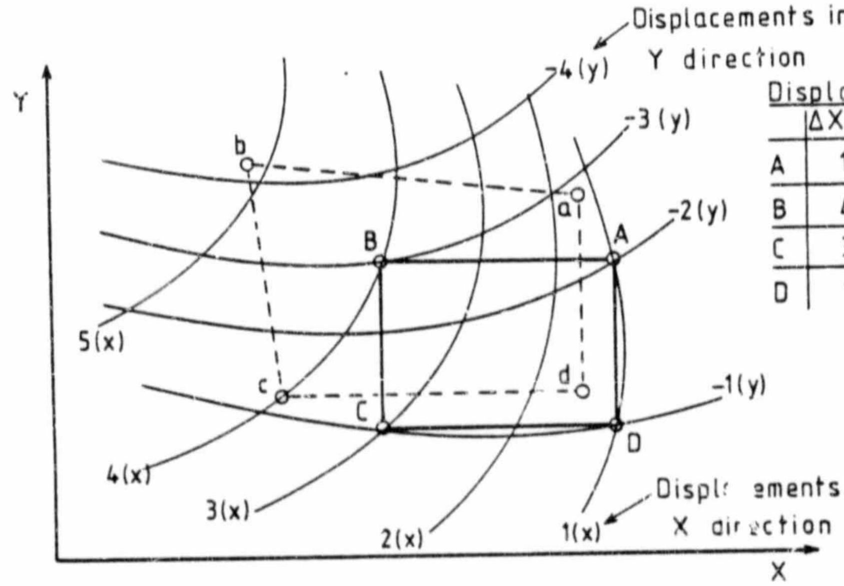

Displacements	$\Delta X=u$	$\Delta Y=v$
A	1	-2
B	4	-3
C	3	-1
D	1	-1

Figure D.2

Use of contour diagrams to obtain displacements at nodes a b c d represent sand grains at their initial positions. A B C D represent the grain positions when displaced by the amou :s indicated by the contours (a grain initially at b, for example, has moved 3 units in the y direction and 4 units in the X direction to arrive at B).

Using the node displacement data, the computer program initially determined the values of the alpha vector in the displacement matrix by applying the Gaussian elimination technique with a 3 cycle refinement routine as discussed by Ralston and Rabinowitz (1978). Radial strain components were then obtained at each node by substituting the alpha vector into the radial strains matrix equation. Because most nodes were common to at least 2 and usually more elements of the grids, the average strain values at each node had to be determined from the values obtained for each common element. Where triangular elements occur in the grid, they were treated as if they were rectangular with one pair of nodes being given the same co-ordinates.

It is considered that over most of the soil displacement field, the finite element mesh dimensions selected were sufficiently fine for the strain data to be estimated with reasonable accuracy. In areas of high strain gradients (close to the pile shaft and toe) however, only a very fine mesh would suffice and in these regions the strain data may be less accurate than elsewhere.

APPENDIX E

E.1 Significance of Load Data

Although the loads measured in the pile shaft were accurate within the stated ranges, unadjusted, they are not an accurate measure of the soil forces on the pile. This is because interface friction between both the pile shoe (Figure 4.3) and the plastic grout-to-glass separator strip (described in Section 4.6) and the glass front panel of the sand box will have contributed to the recorded load. Estimates of the magnitude of this interface friction component under the conditions of the various load tests are presented in the following. The estimates are developed from simplified loading conditions using simple statics.

It is known that under some loading conditions, the orientation of the axes of principal strain increments do not necessarily coincide with the orientations of the corresponding axes of principal stress. (Roscoe [1970], Arthur et al [1977], Arthur et al [1980], Wood [1980]). In particular, where boundary conditions which impose mecahnical restraints on strain movements exist, the angular deviation may be of the order of 15^{o} (Arthur et al [1977]). Considered in isolation, therefore, the diagrams showing principal strain directions in the sand surrounding the model pile cannot be relied on to indicate the directions of the forces acting in the soil. Deviation of strain increment and stress direction is likely to be greatest along the pile/soil interface, and it is suggested that the strain data close to the pile can only be used to obtain a general indication of stress direction.

In view of the possible deviation of strain increment and stress orientation, various assumptions have been made in the following regarding the friction developed along the pile/soil interface.

E.2 Friction between Pile Shoe and Glass Panel

The accuracy of all of the recorded load data will have been influenced by friction between the pile shoe and the glass front panel of the sand box.

The pile shoe moving into the soil can be considered analogous to a block of sand sliding over a smooth steel surface, where the block possesses the properties of the sand displaced by the passage of the pile shoe. Figure E.1 shows the various force components applicable to the friction block analogy. In this diagram:

Fh	=	soil resistance to horizontal displacement
Fvh	=	vertical force required to overcome Fh
Fs	=	friction between pile shoe and soil

Fvs = vertical force required to overcome Fs

Fvv = soil resistance to vertical displacement

Fn = force acting normal to the glass panel

Fvn = vertical force required to overcome friction between the pile shoe and glass panel

Fvt = total applied force required to cause pile penetration

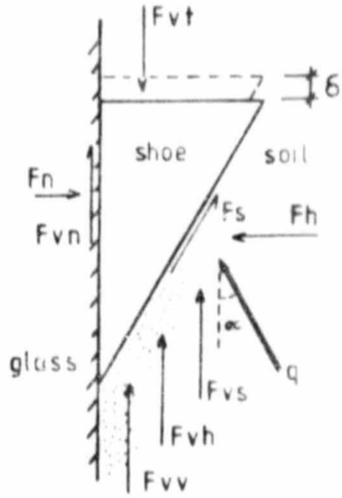

FIGURE E.1a: Section through shoe.

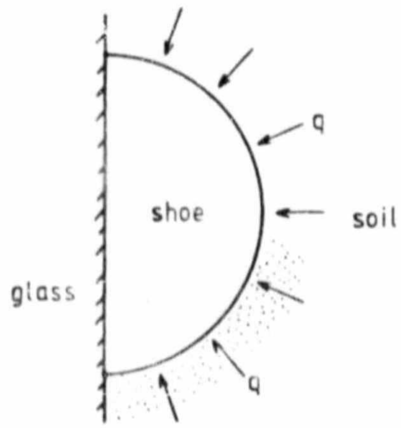

FIGURE E.1b: Plan of shoe.

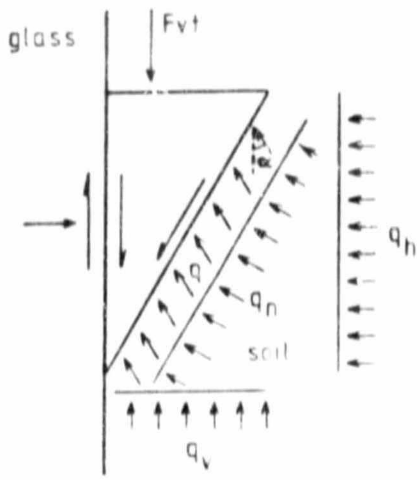

FIGURE E.1c: Stress components.

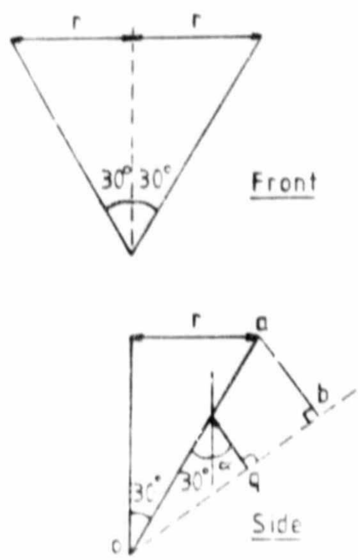

FIGURE E.1d: Projection planes.

FIGURE E.1: Summary of force and stress components resisting penetration of the model pile shoe.

The soil forces acting on the curved surface of the pile shoe may be resolved for simplicity into a resultant uniform stress, q, acting on the shoe surface at some angle α , measured from a vertical axis (see Figure E.1c). Various equations expressed in terms of this uniform stress may be developed to determine the force components, and in particular the magnitude of 'Fvn' relative to the total applied vertical force.

The vertical forces acting on the pile shoe may be summed,

$$Fvt = Fvh + Fvs + Fvv + Fvn \qquad (E-1)$$

F'vv may be written as the sum of the vertical forces due to soil action on the curved portion of the shoe. Thus,

$$F'vv = Fvh + Fvs + Fvv \qquad (E-2)$$

Hence,

$$Fvt = F'vv + Fvn \qquad (E-3)$$

The magnitude of the force F'vv may be found as follows:

Total force on curved surface of shoe = q.Ac

where Ac = surface area of the curved portion of the shoe cone.

The vertical component, F'vv, of this total force is then,

$$F'vv = q.Ac.\cos\alpha \tag{E-4}$$

Fvn, the friction between the pile shoe and the glass face panel, may be found as follows (refer to Figure E.1d):

Fn, derived from the total horizontal force on the shoe cone, is that component acting normal to the face of the glass panel. The area over which Fn acts is the triangular front face of the cone, the area of which may be given as,

$$\text{Area of front face of cone} = \frac{r^2}{\tan 30}$$

If this surface is projected onto plane oa lying along the rear of the cone, the projected area becomes,

$$\text{Projected area on plane oa} = \frac{r^2}{\tan 30} \cdot \frac{1}{\cos 30}$$

When projected onto a plane lying along ob this area becomes,

$$\text{Projected area on plane ob} = \frac{r^2}{\tan 30} \cdot \frac{1}{\cos 30} .\cos\alpha$$

The uniform stress, q, acts perpendicular to ob. It also acts radially on the curved surface of the shoe cone. The force resulting from q acting on the plane projected to ob rather than on the curved surface will be less than the total force on the cone by the amount,

$$\frac{1/2.\pi r^2}{2r.r} = 0,79$$

and the resultant force acting on the area projected to plane ob will then be,

$$= \frac{0,79.q.r^2 .\cos \alpha}{\tan 30.\cos 30} \qquad \text{(E-5)}$$

The horizontal component of this force, Fn, is that force which pushes the cone against the glass face panel.

$$\text{ie} \qquad Fn = \frac{0,79.q\ r^2 .\cos \alpha.\sin \alpha}{\tan 30.\cos 30} \qquad \text{(E-6)}$$

The resistance to sliding between the cone and the glass, Fvn, is obtained from Fn.

$$Fvn = Fn.\tan \theta sg \qquad \text{(E-7)}$$

Using equation E-3 the friction between the pile shoe and the glass face may then be obtained as a proportion of the total applied vertical load.

$$\frac{Fvn}{Fvt} = \frac{Fvn}{Fvn + F'vv} \qquad (E-8)$$

If α and θsg are known, equation E-8 may be solved.

Tests by the writer showed that the friction angle, θsg, between the pile shoe and the release agent coated glass face panel was about 14°, and that the dynamic and static friction angles were similar.

ie for both impact and static loading $\theta sg = 14^{\circ}$

It is clear that the angle α must lie within the range $0 < \alpha < 90^{\circ}$. It appears reasonable to suggest that under the plastic strain conditions which developed close to the moving pile toe, the direction of the resultant stress q, was likely to have been aligned approximately along the trajectory of the displaced sand grains. An implication of this assumption with regard to the Coulomb failure concept that slip occurs at an angle of $45 + \theta/2$ degrees to the major principal stress direction, is that slip on the surface of the pile did not occur on a plane of maximum stress obliquity.

If this assumption is applied to the present analysis, then the data in Table 6.3 (pg 6.23) suggest that during impact, the stress resultant, q, was inclined at an average angle of about 40° from the vertical. During static loading, however, the data in Table 6.4 suggest that the average angle was about 30°.

ie During impact $= 40^{\circ}$

During static loading $\alpha = 30^{\circ}$

If the above values of α and θsg are substituted into equation E-8, it emerges that the proportion of the load developed on the pile toe by friction between the pile shoe and the glass panel was as follows:

During impact ($\alpha = 40^{\circ}$) glass friction = 7% of toe load

During static loading ($\alpha = 30^{\circ}$) glass friction = 6% of toe load

The strain data suggest that the horizontal load acting on the shoe collar was probably significantly less than that acting on the conical shoe. It is considered therefore that friction between the pile shoe and glass panel may reasonably be expected to have been of the order of 10% of the measured (interpolated) toe load - slightly greater than that calculated for the conical shoe alone.

E.3 Friction on the Plastic Separator Strip during Installation

During pile installation, the plastic separator strip used to isolate the grout column in the pile shaft from the glass front panel, moved down into the sand box in

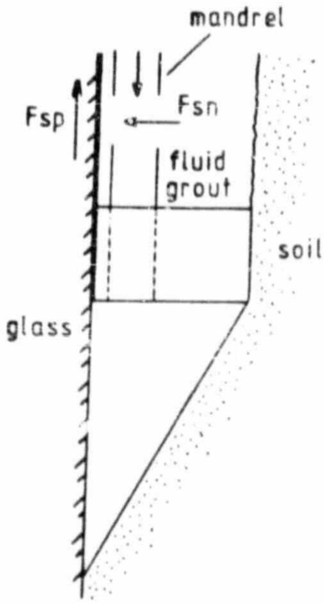

FIGURE E.2a: Plastic separator strip load.

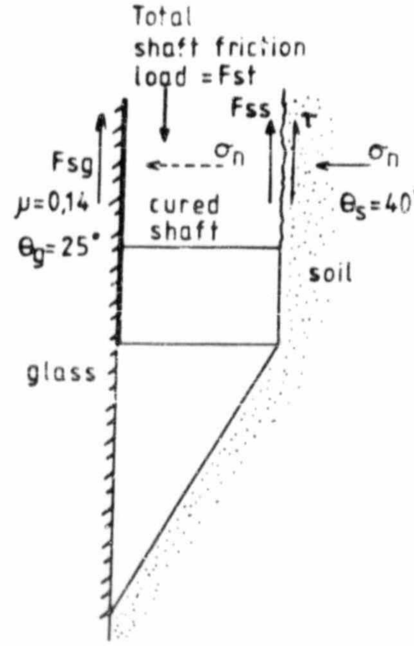

FIGURE E.2b: Loads on the cured shaft.

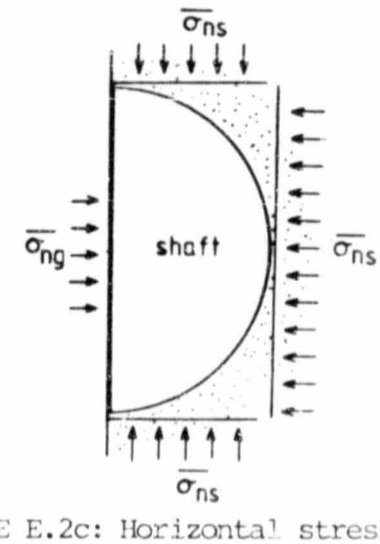

FIGURE E.2c: Horizontal stress on the pile shaft.

FIGURE E.2: Summary of friction load components in the grout column and on the pile shaft.

unison with the drive mandrel and the pile shoe. Any restraint on the free movement of the strip, which was fixed to the pile shoe, would have imposed a load on the pile shoe in addition to the resistance imposed by the soil. The magnitude of this restraint can again be estimated using a friction block analogy.

The horizontal load acting on the plastic strip can be estimated from the hydrostatic pressure exerted by the grout column located along the inner surface of the strip. It was noted in Section 4.6 that the density of the cured grout was 2100 kg/m^3. The submerged unit weight was therefore about 11 kN/m^3. At the depth at which static load measurements were made on the pile shoe immediately following pile installation, the grout column was about 870mm deep. The average horizintal force, Fsh, acting on the 60mm wide strip can then be calculated as 250N. Tests carried out by the writer indicated that under simulated experimental conditions the plastic to glass sliding friction coefficient was about 0,14 and the static coefficient was about 0,17. (This is similar to data for plastic to plastic friction coefficients for polyamide plastics of 0,1 to 0,3 given by Chong [1977].) The additional load, Fss, imposed on the pile shoe from this source can accordingly be estimated as (see Figure E.2a):

Fss = Fsh 0,14 = 250 x 0,14

≈ 35N to 42,5N

Viscous drag from the rising grout column and contamination by sand and cement of the glass plastic interface would likely have added to the calculated friction, and it is suggested that a reasonable estimate of the strip load would be of the order of 50N to 60N.

E.4 Friction between Pile Shaft and Glass Panel

An exercise similar to that performed for the pile shoe can be carried out to estimate the proportion of the measured shaft load contributed by friction between the pile shaft and the glass face panel.

Load shed by friction along the pile shaft was contributed from two sources. These included frictional resistance developed by shear between the shaft and the soil, and between the shaft and the glass panel. The magnitude of this shear resistance, τ, is generally considered to be the product of the normal stress and the friction coefficient, tan θ.

$$\tau = \sigma_n . \tan \theta$$

Expressed in terms of average normal stresses, σn, and friction coefficients, the total shaft resistance, Fst, can be written as the sum of the soil, Fss, and glass, Fsg, friction components:

$$Fst = Fss + Fsg = \overline{\sigma ns} \tan \theta_s . As + \overline{\sigma ng} \tan \theta g . Ag \qquad (E-9)$$

where As = surface area of the pile shaft in contact with the soil, Ag = surface area of the pile shaft in contact with the glass and the subscript 's' refers to shaft/soil interaction, while the subscript 'g' refers to glass/shaft interaction. In equation (E-9) the horizontal stresses will be equal, (see Figures E.eb&c):

$$\overline{\sigma_{ns}} = \overline{\sigma_{ng}}$$

The ratio of total shaft friction to glass/shaft friction, Fst/Fsg, may thus be obtained as:

$$\frac{F_{st}}{F_{sg}} = \frac{\tan \theta_s . A_s}{\tan \theta_g . A_g} + 1$$

which, on substituting suitable values for As and Ag, becomes:

$$\frac{F_{st}}{F_{sg}} = \frac{\tan \theta_s . \pi}{\tan \theta_g . 2} + 1 \qquad \text{(E-10)}$$

It remains therefore to identify suitable values of θ_s and θ_g.

It has been observed that soil densification occurred close to the pile shaft during pile installation. It has also been observed that the shaft grout bonded to the soil boundary layer on curing. In recognition of these observations, it is suggested that, for the purpose of this analysis, a reasonable estimate of the average soil/shaft friction angle is $\theta s = 40^{\circ}$.

It was recorded in Section E.3 that the friction coefficient between the plastic separator strip and the glass panel was 0,14. Due to the presence of small amounts of leaked grout and scattered sand grains which contaminated the shaft/glass interface, however, the friction coefficient applicable to the static load tests would have been somewhat higher. Mitchell (1977, p.311) lists friction coe.ficients for various silicate minerals. With reference to this data, and in the absence of any measurements of the shaft/glass friction co-efficient, it is suggested that a possible friction angle could have been of the order of $\theta g = 25^{\circ}$.

On substituting the above values of θg and θs into equation (E-10), it emerges that friction between the pile shaft and glass face panel may have contributed about 26% of the measured shaft friction load. A friction correction factor of 0,26 has accordingly been used in estimating pile/soil interface shear stresses in Chapter 6.

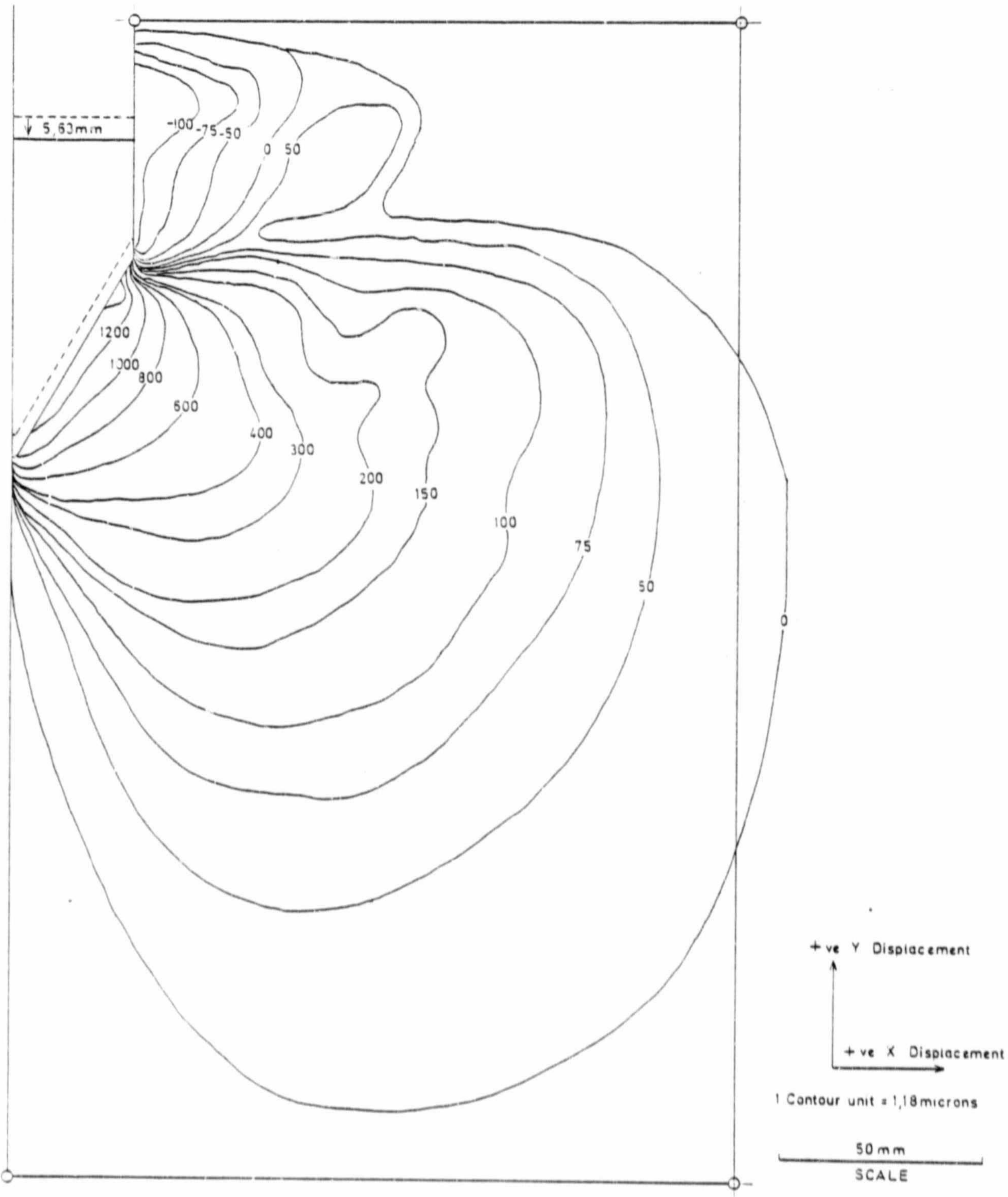

FIGURE 5.2 Horizontal (X axis) sand grain displacements. Plates 1-2 Dynamic.

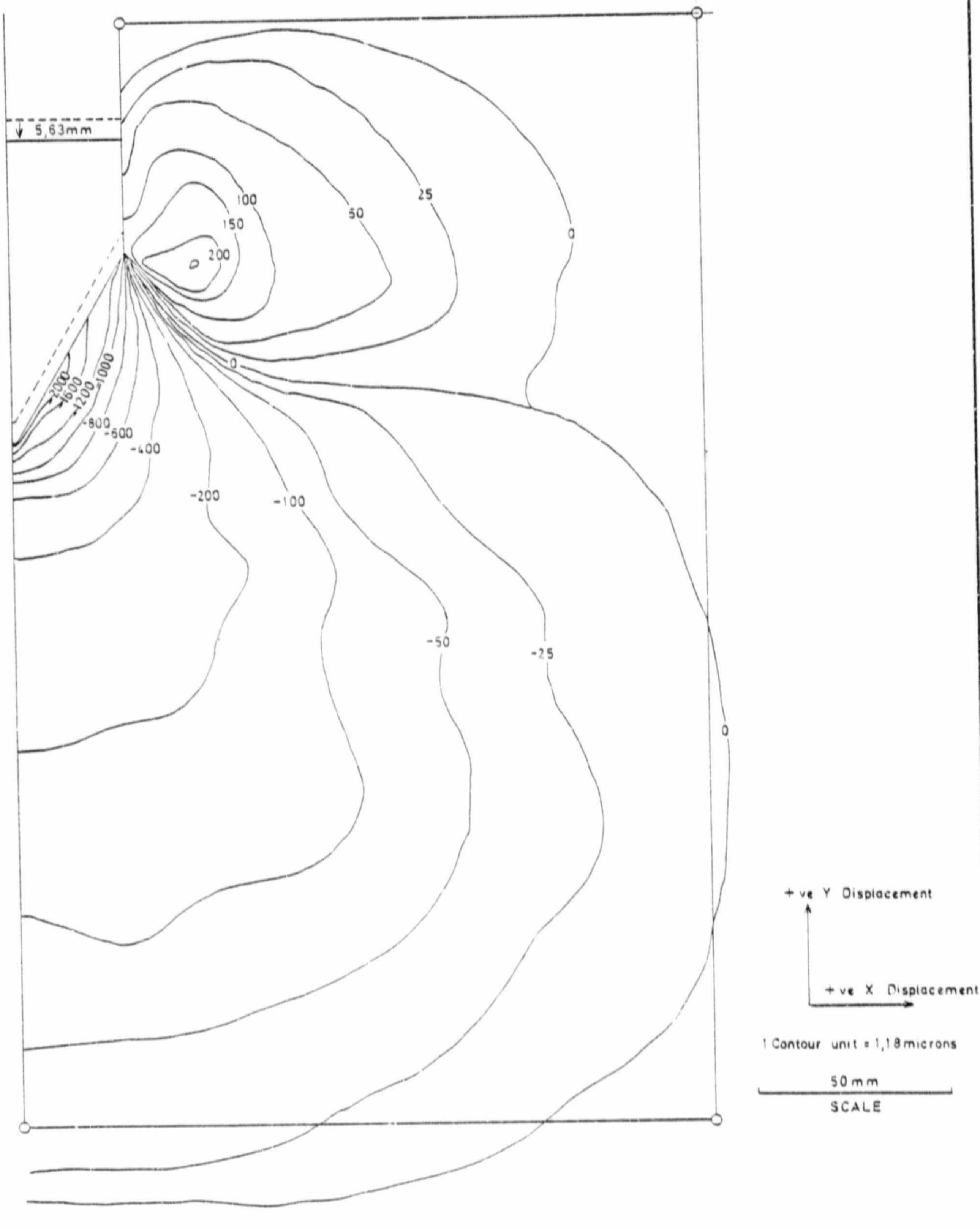

FIGURE 5.3 Vertical (Y axis) sand grain displacements. Plates 1-2 Dynamic.

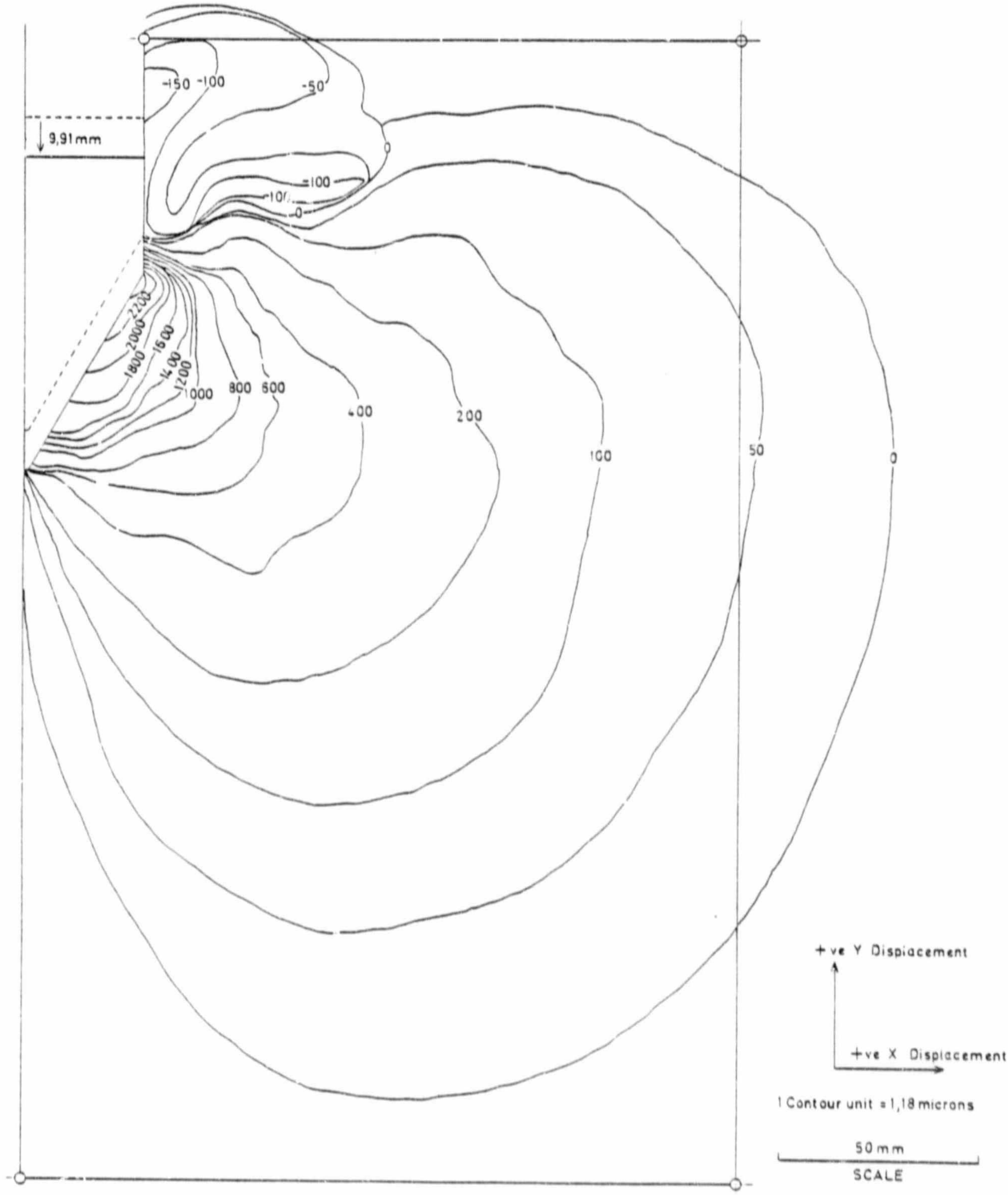

FIGURE 5.4 Horizontal (X axis) sand grain displacements. Plates 1-3 Dynamic.

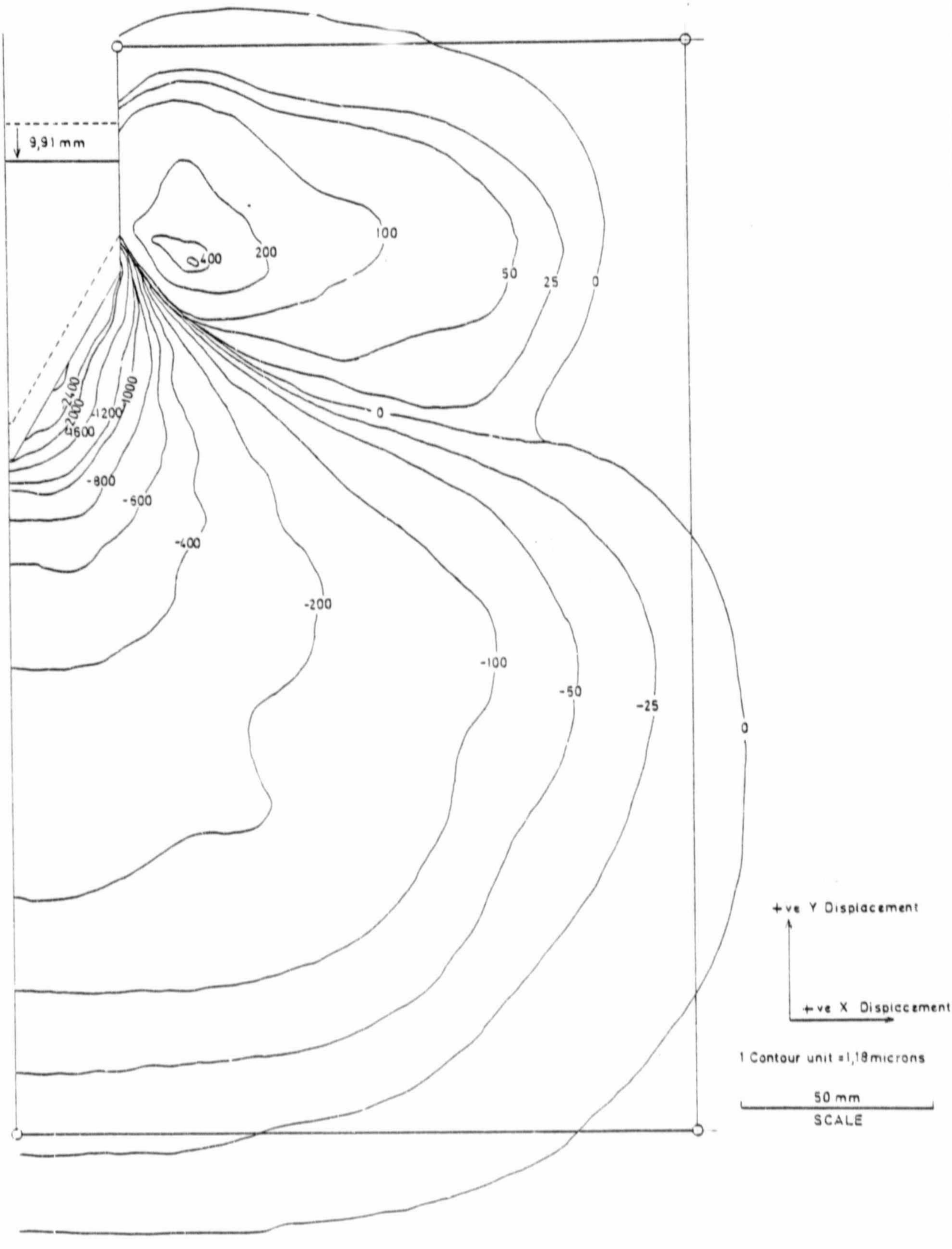

FIGURE 5.5 Vertical (Y axis) sand grain displacements. Plates 1-3 Dynamic.

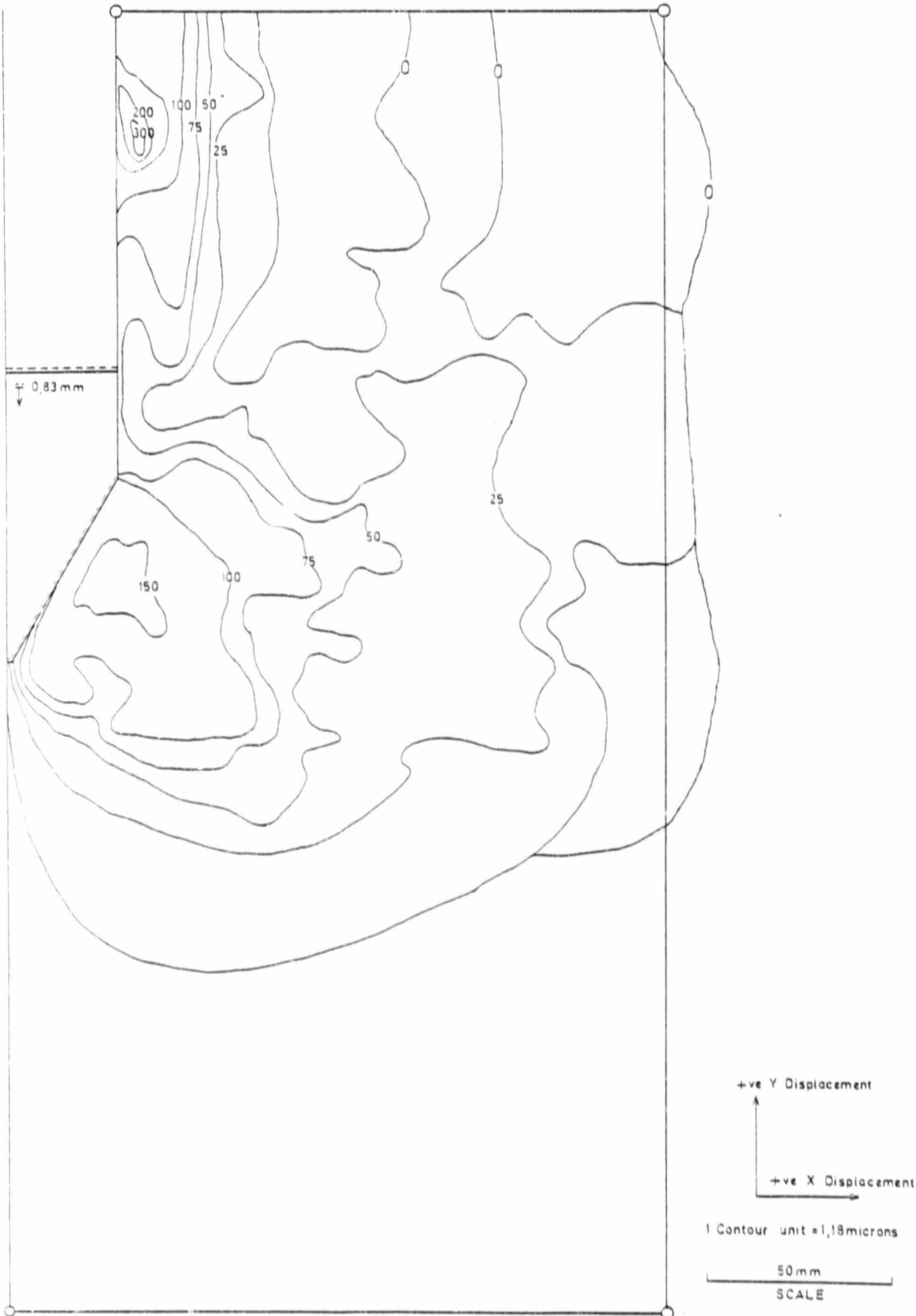

FIGURE 5.10 Horizontal (X axis) sand grain displacements

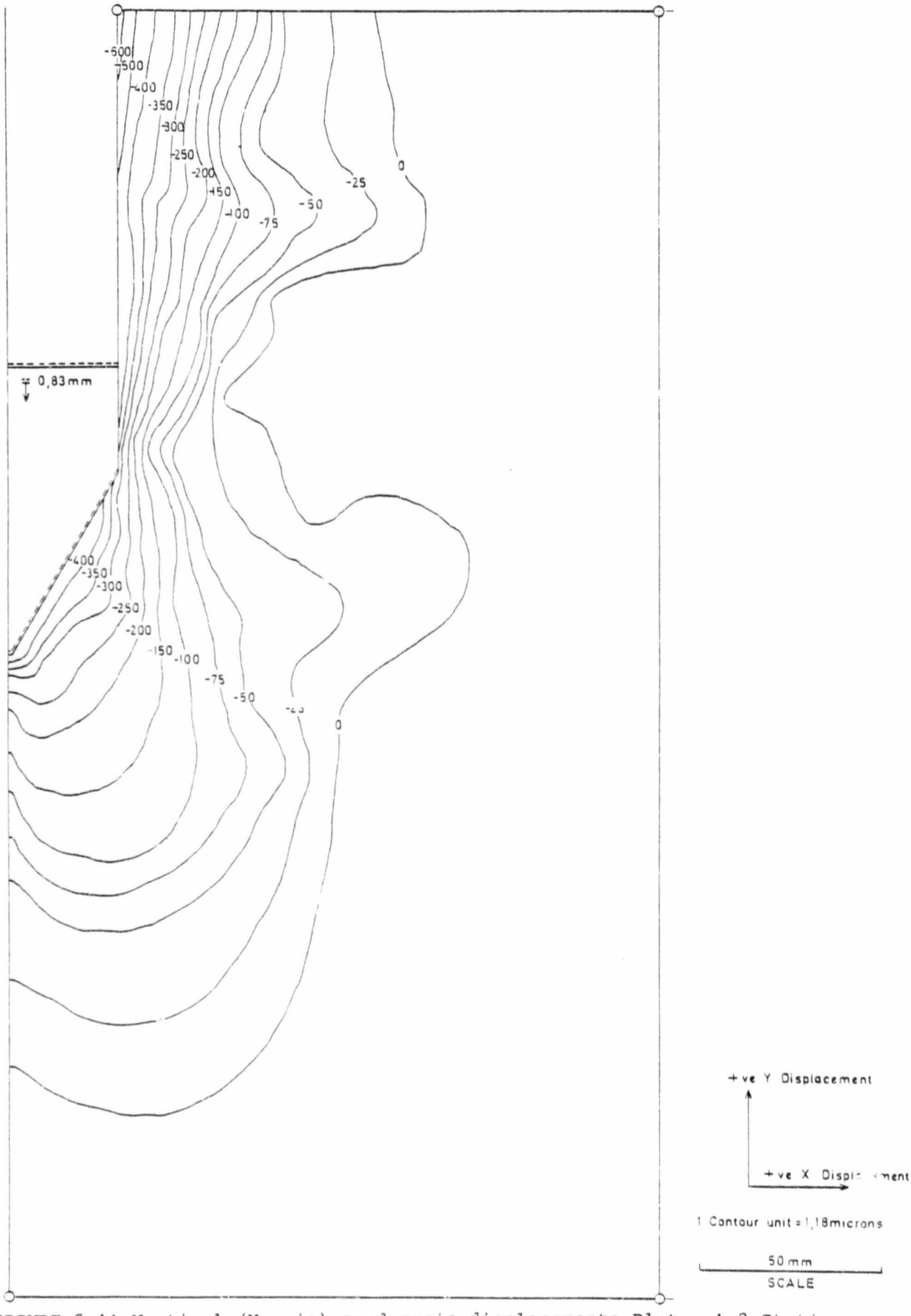

FIGURE 5.11 Vertical (Y axis) sand grain displacements.Plates 1-2 Static.

Pocket 7

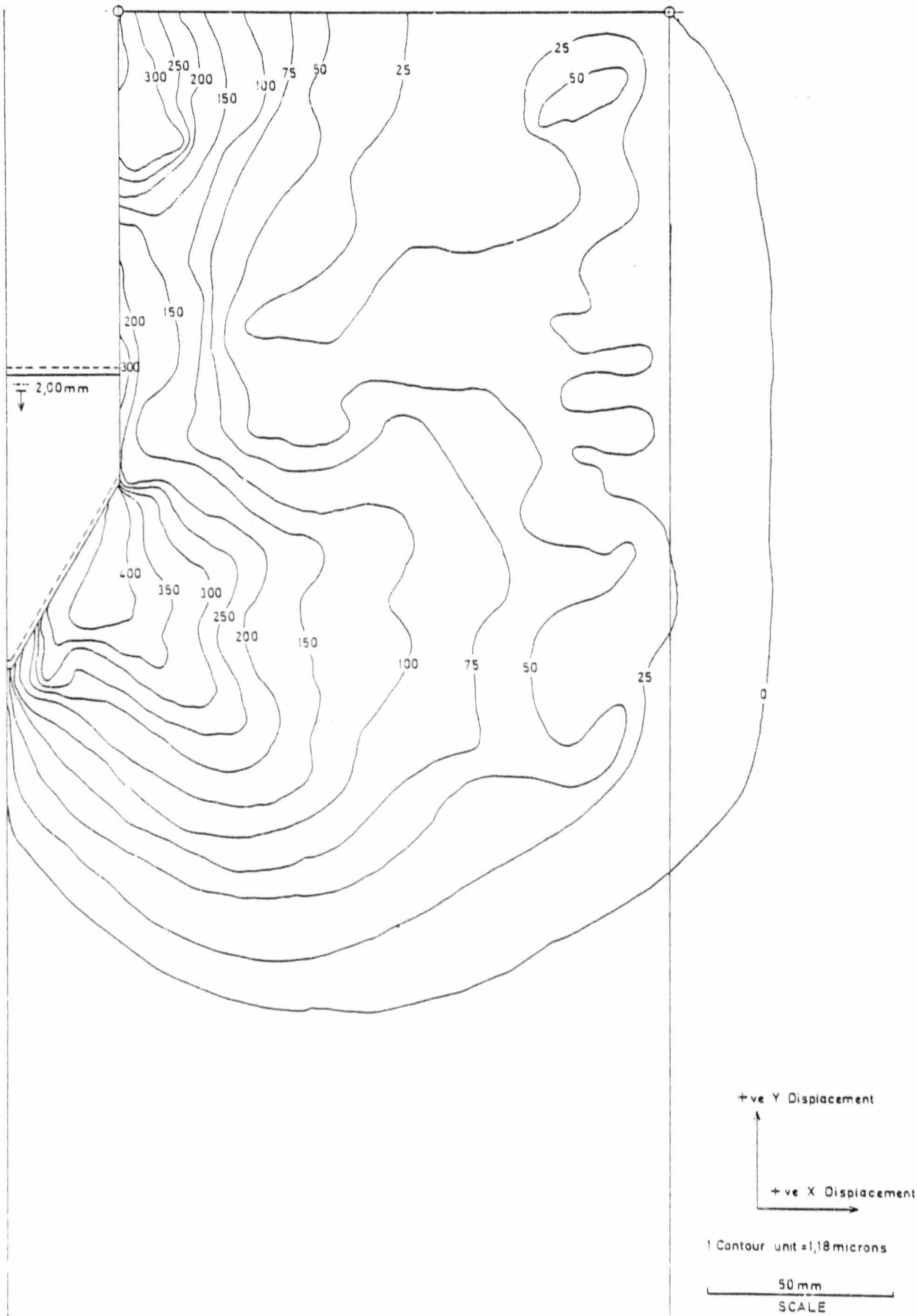

FIGURE 5.12 Horizon[illegible]axis) sand grain displacements. Plates 1-3 Static.

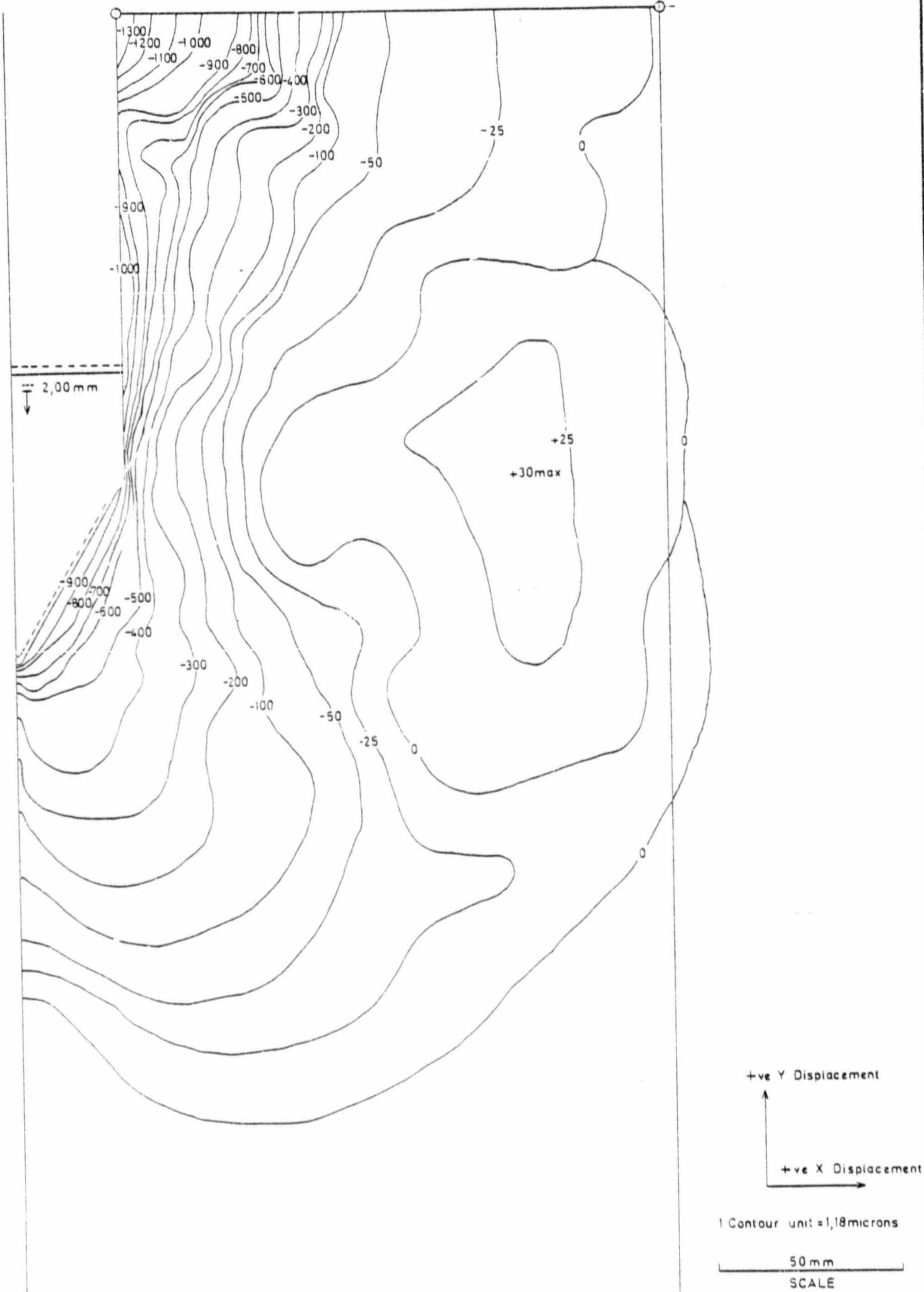

FIGURE 5.13 Vertical (Y axis) sand grain displacements. Plates 1-3 Static.

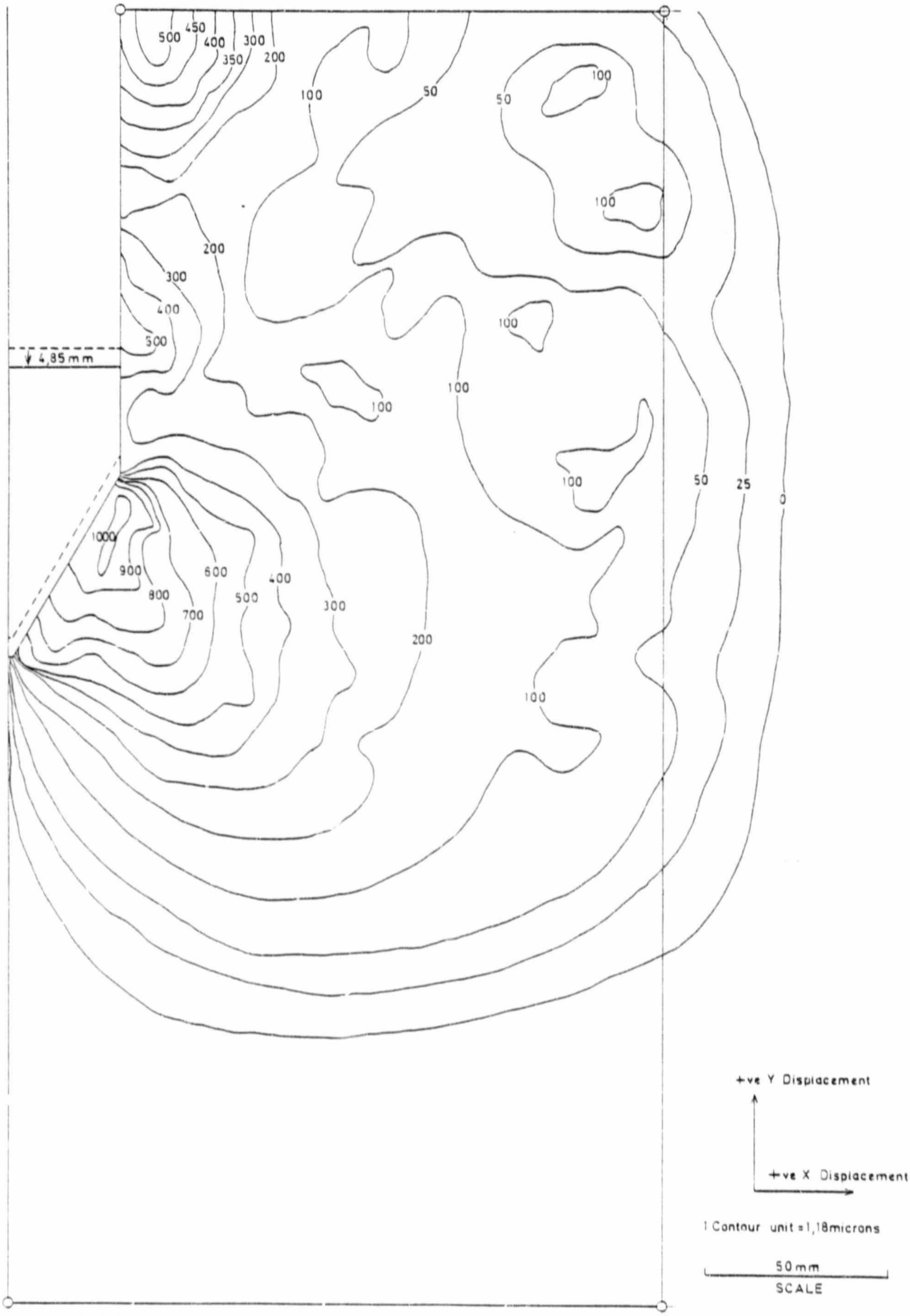

FIGURE 5.14 Horizontal (X axis) sand grain displacements. Plates 1-4 Static.

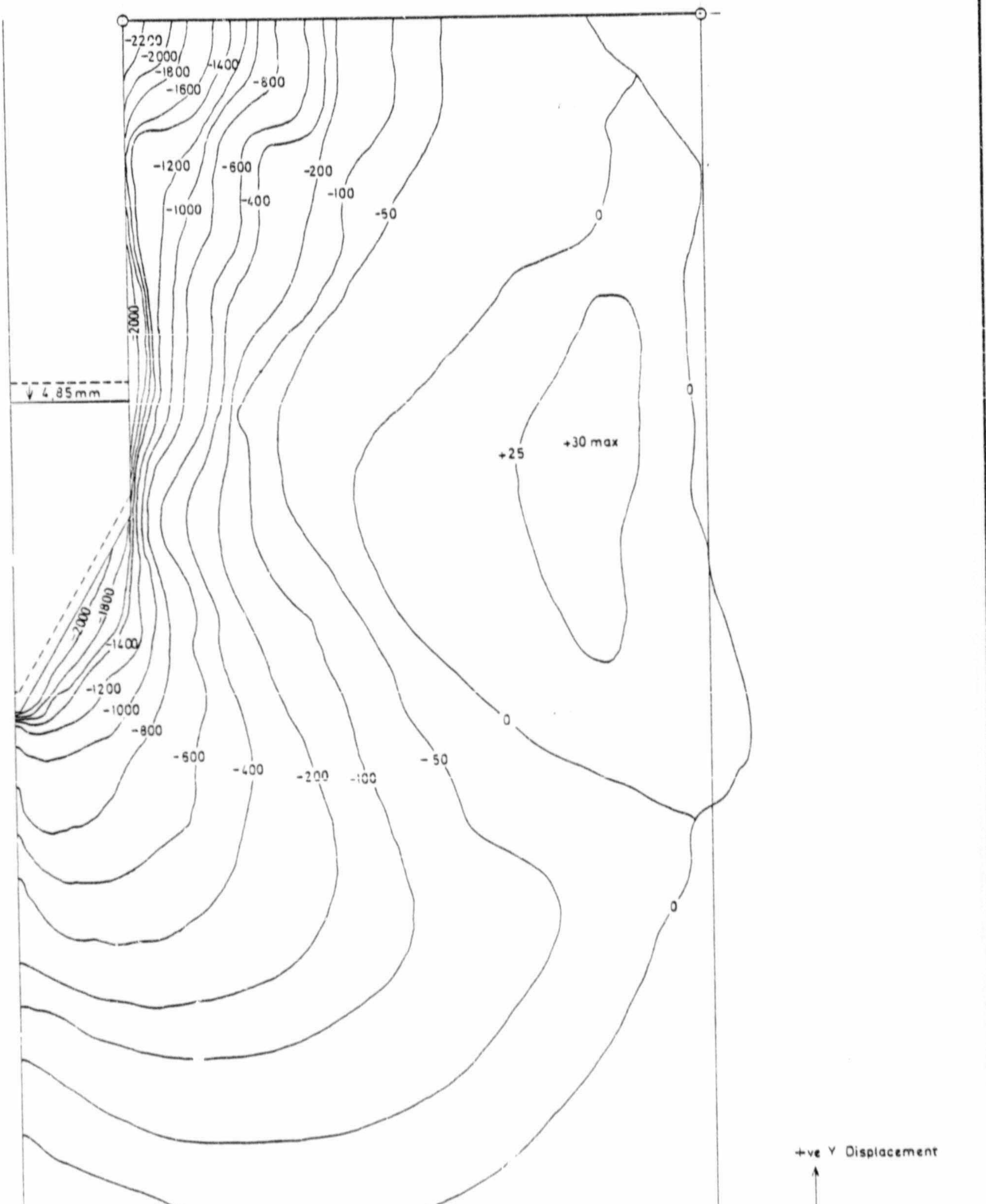

FIGURE 5.15 Vertical (Y axis) sand grain displacements. Plates 1-4 Static.

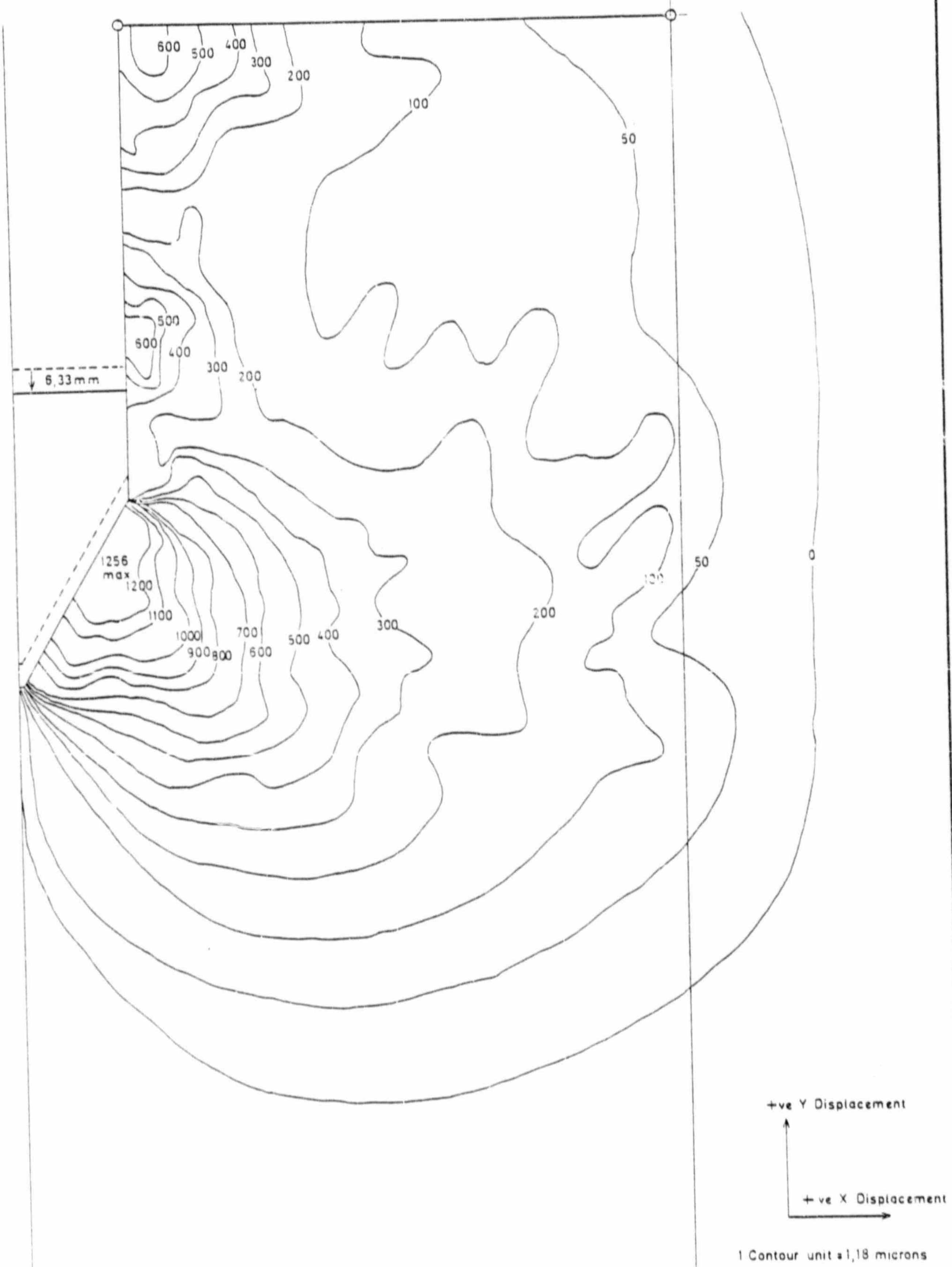

FIGURE 5.16 Horizontal (X axis) sand grain displacements. Plates 1-5 Static.

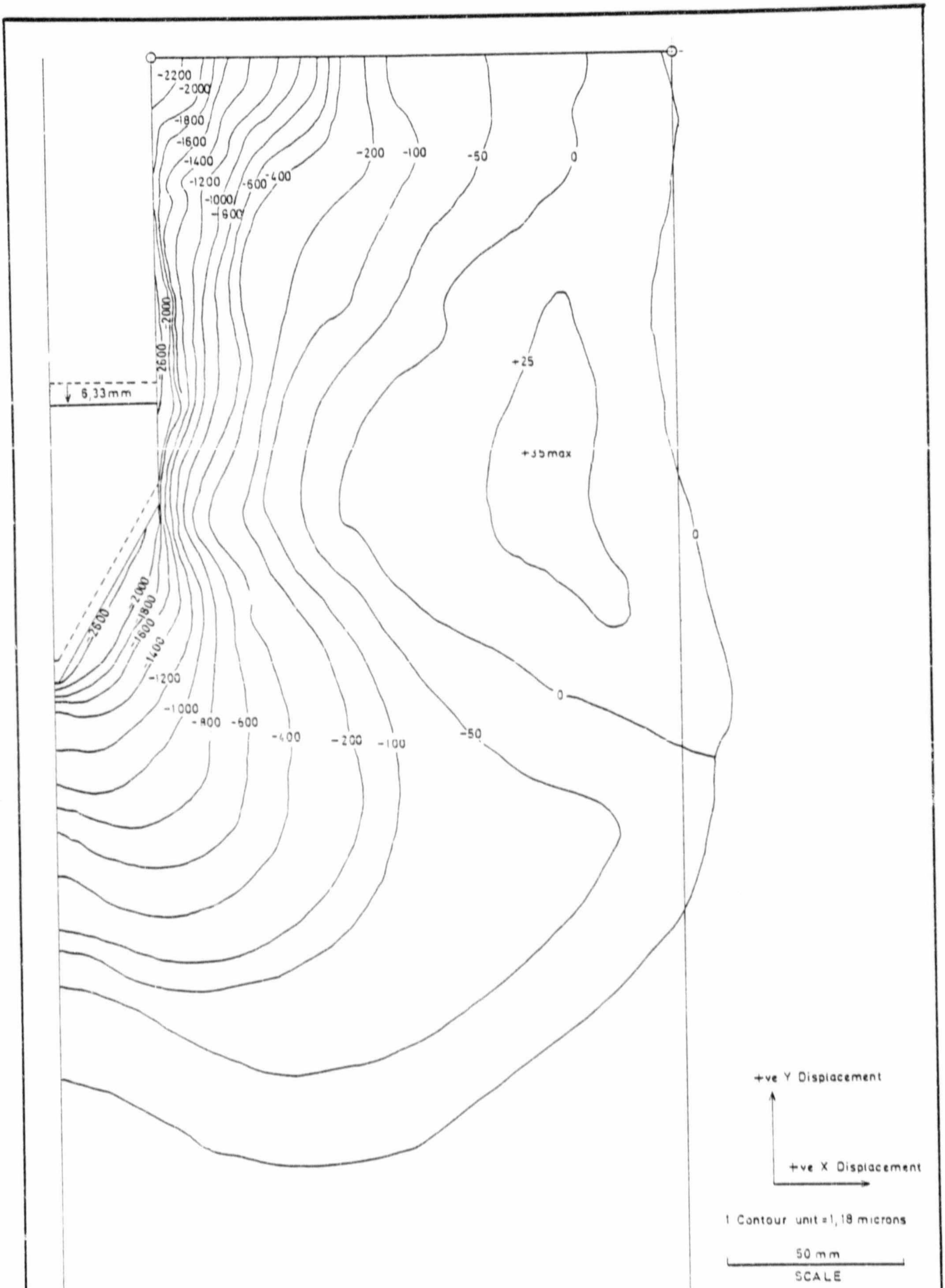

FIGURE 5.17 Vertical (Y axis) sand grain displacements. Plates 1-5 Static.

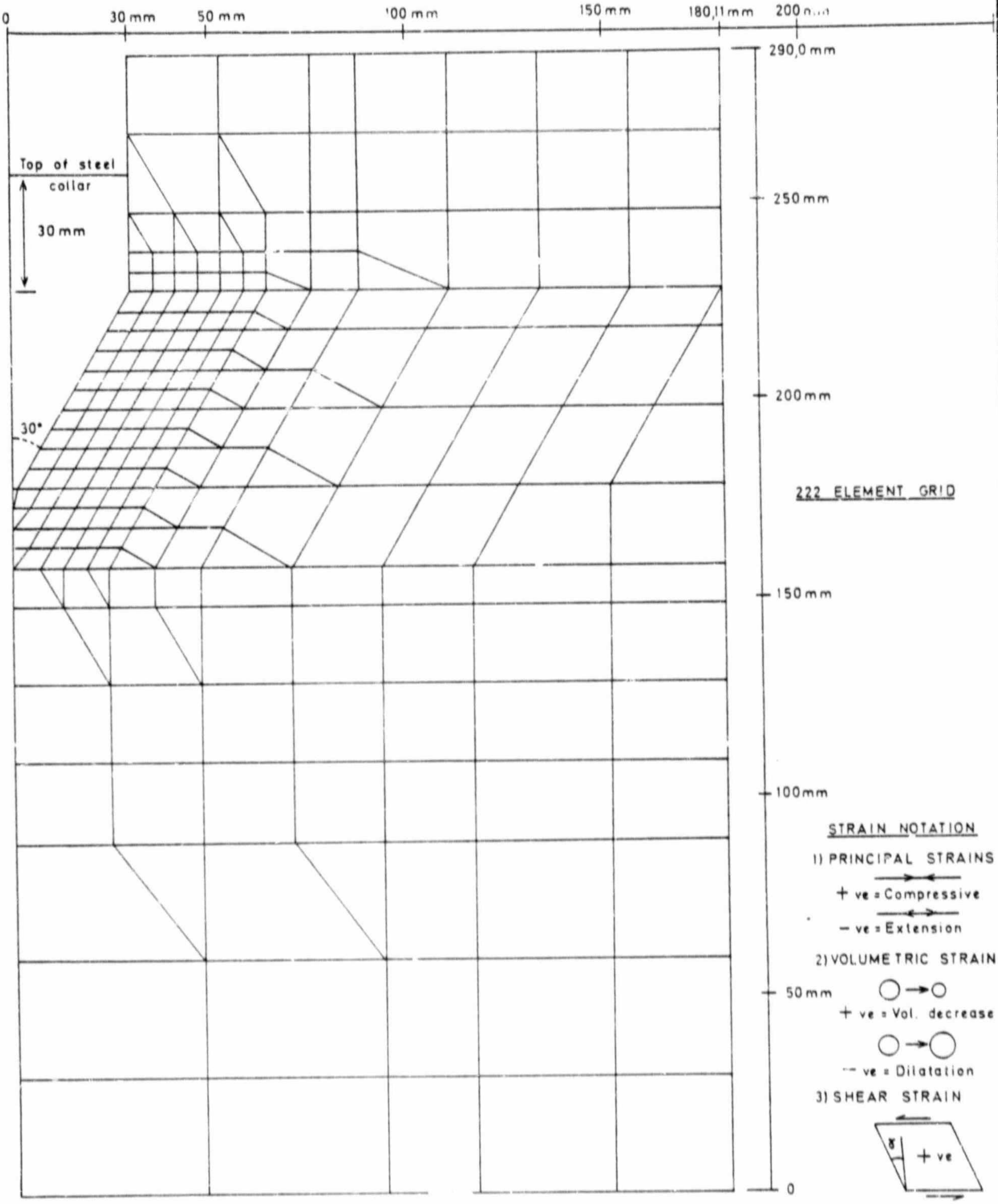

FIGURE 6.7 Rectangular grid used to estimate pile installation soil strains.

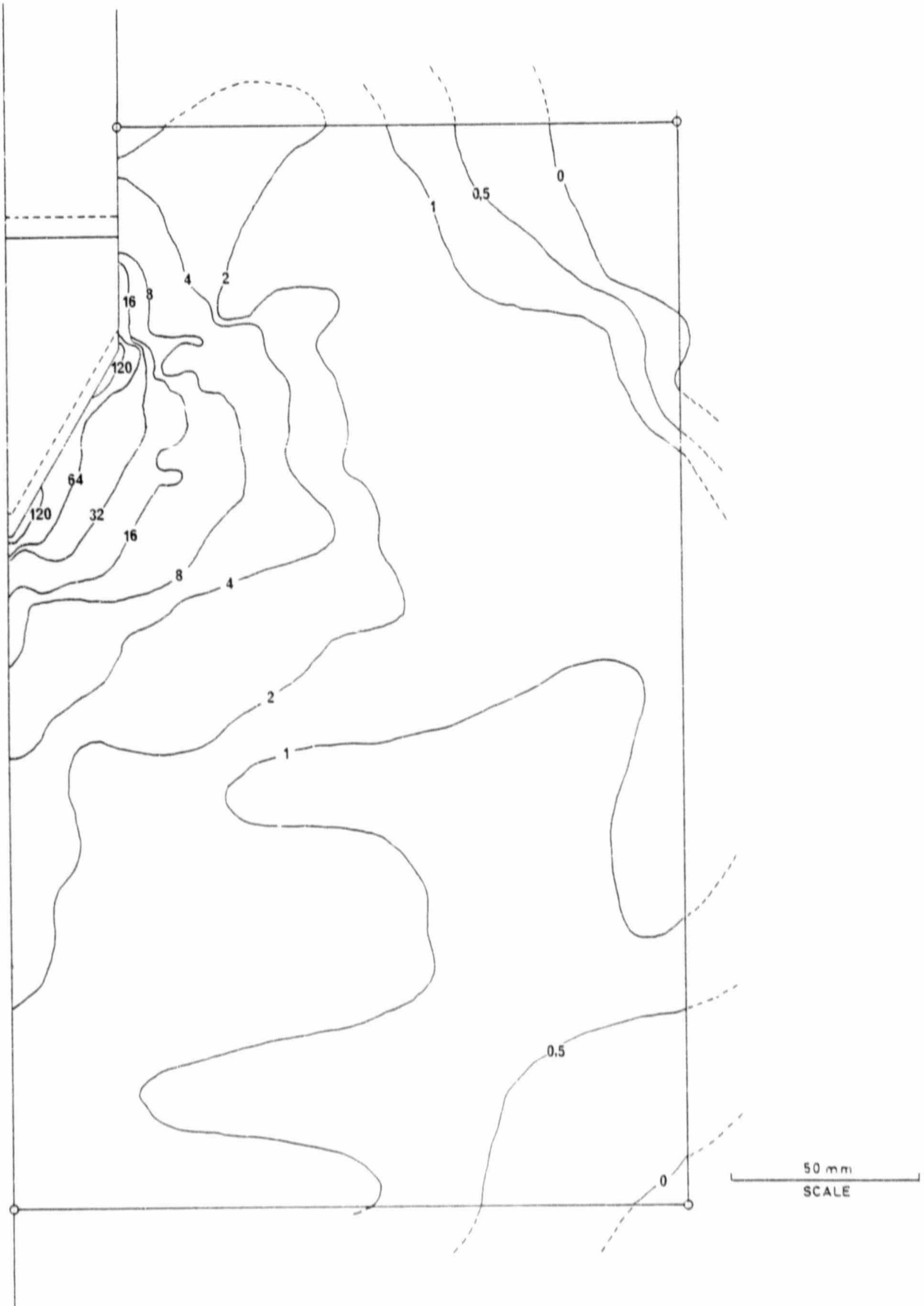

FIGURE 6.8 Major principal strain contours at $10^3 \mu$-strain. Plates 1-2 Dynamic.

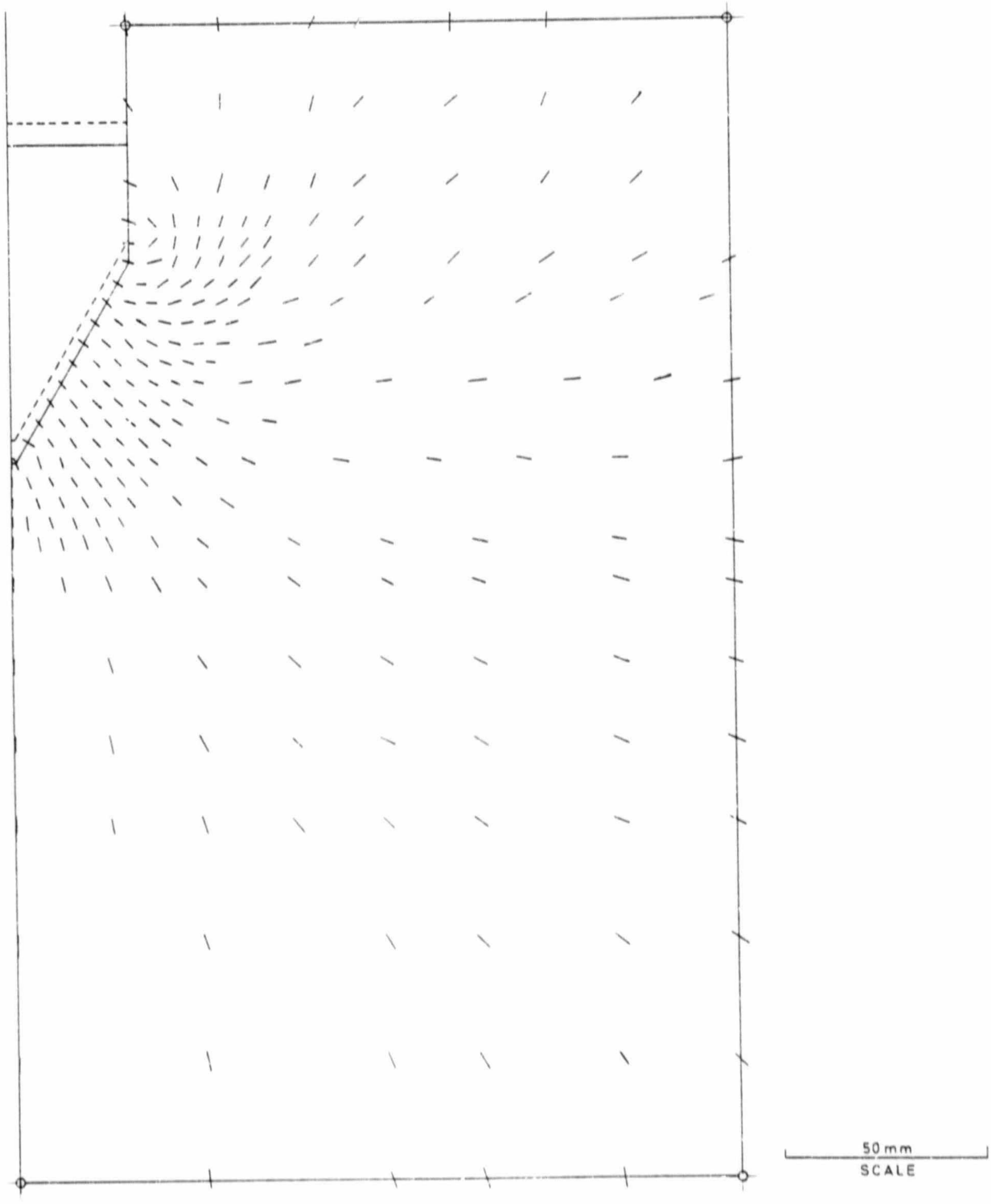

FIGURE 6.9 Major principal strain directions. Plates 1-2 Dynamic.

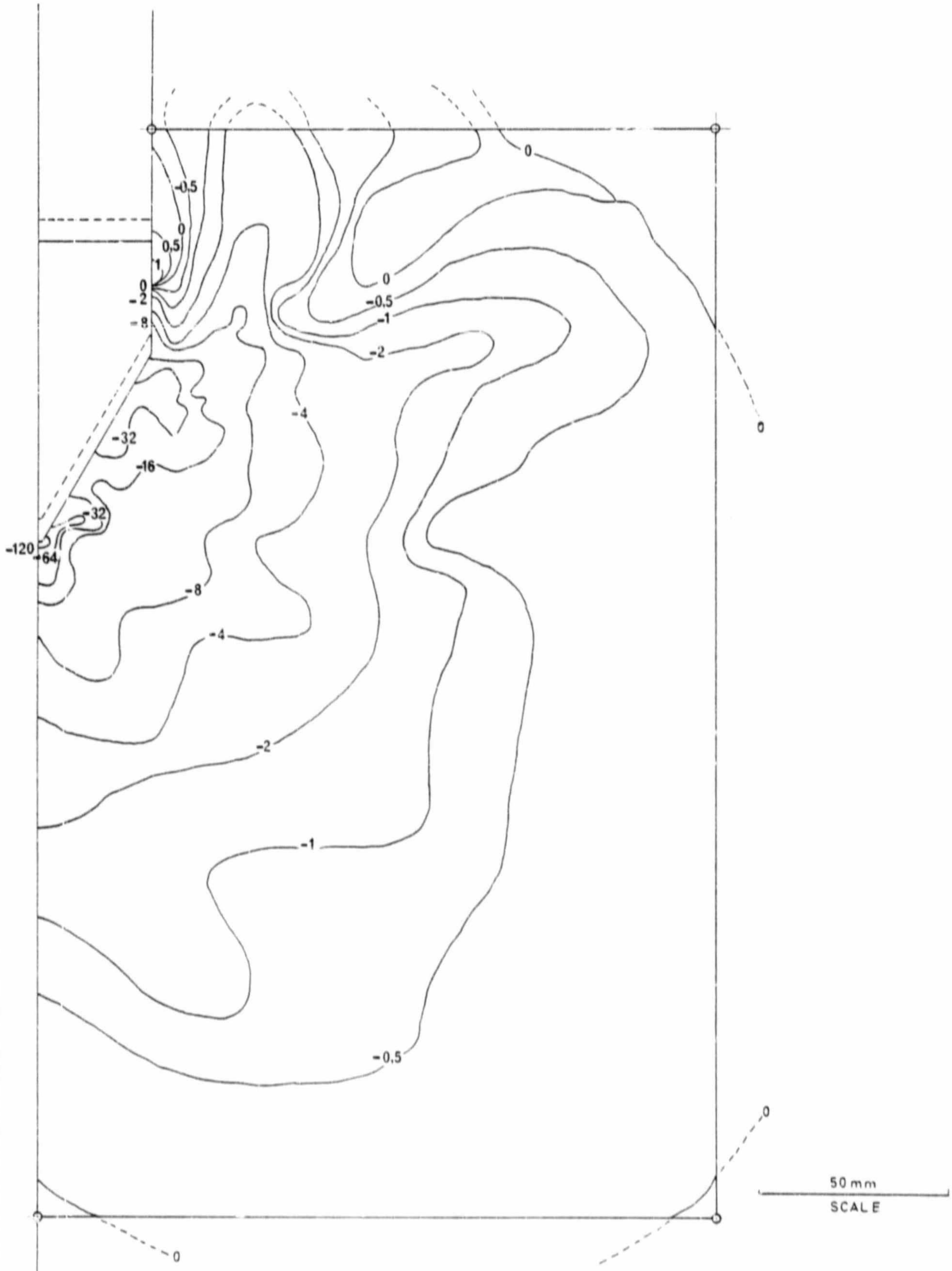

FIGURE 6.10 Minor principal strain contours at 10^3 μ-strain.
Plates 1-2 Dynamic.

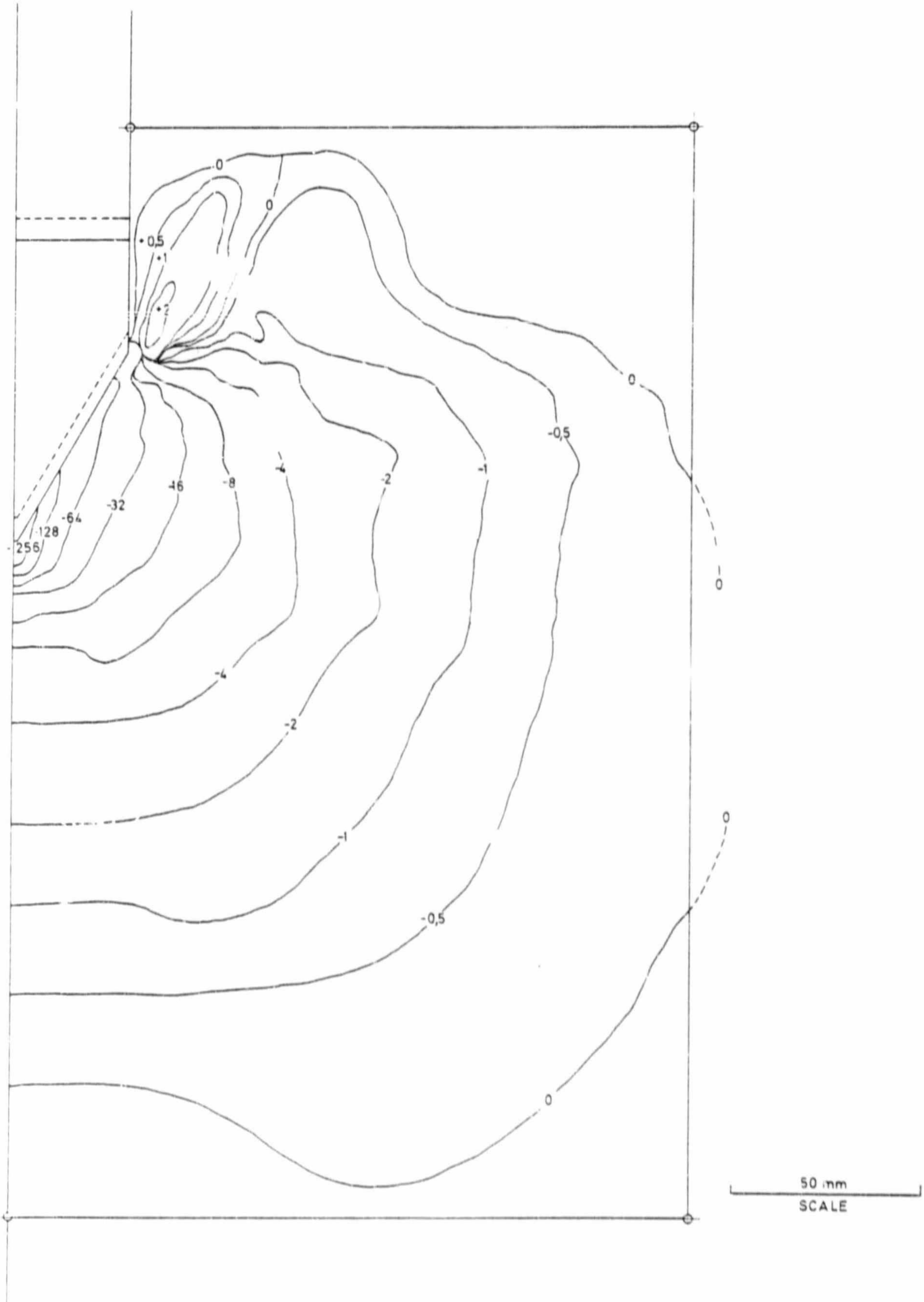

FIGURE 6.11 Circumferential strain contours at $10^3\,\mu$-strain. Plates 1-2 Dynamic.

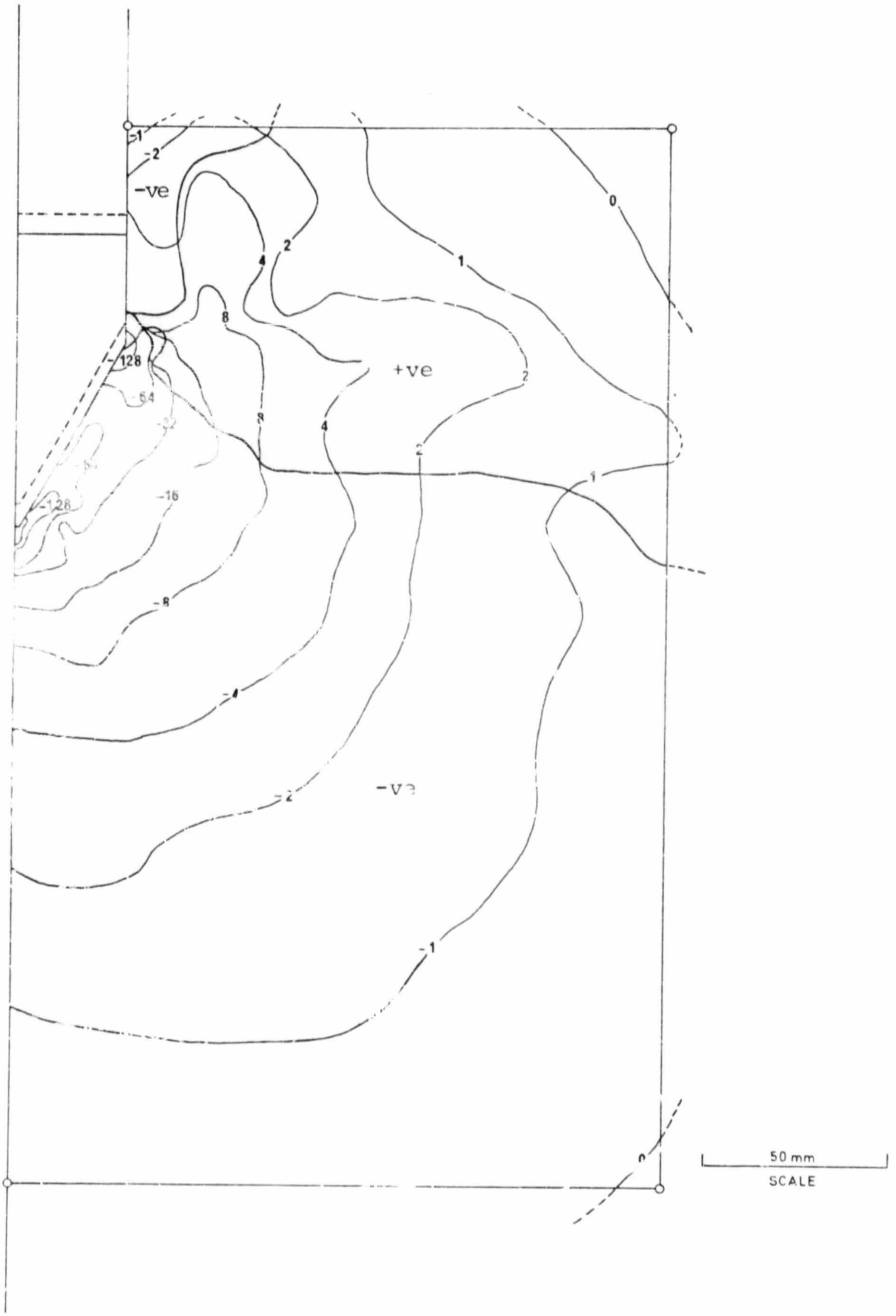

FIGURE 6.12 Maximum shear strain contours at $10^3\mu$-strain. Plates 1-2 Dynamic.

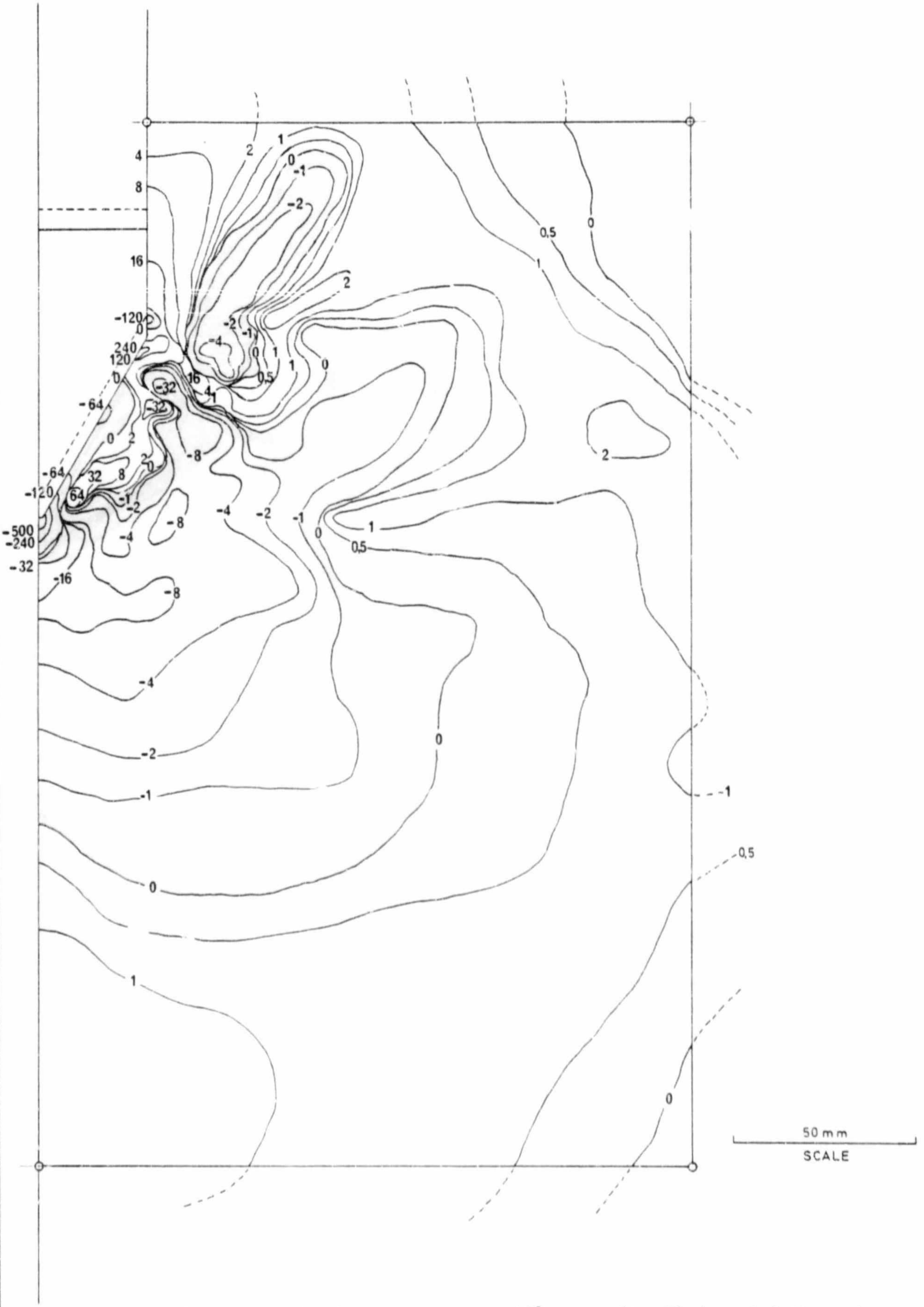

FIGURE 6.13 Volumetric strain contours at 10^3 μ-strain. Plates 1-2 Dynamic.

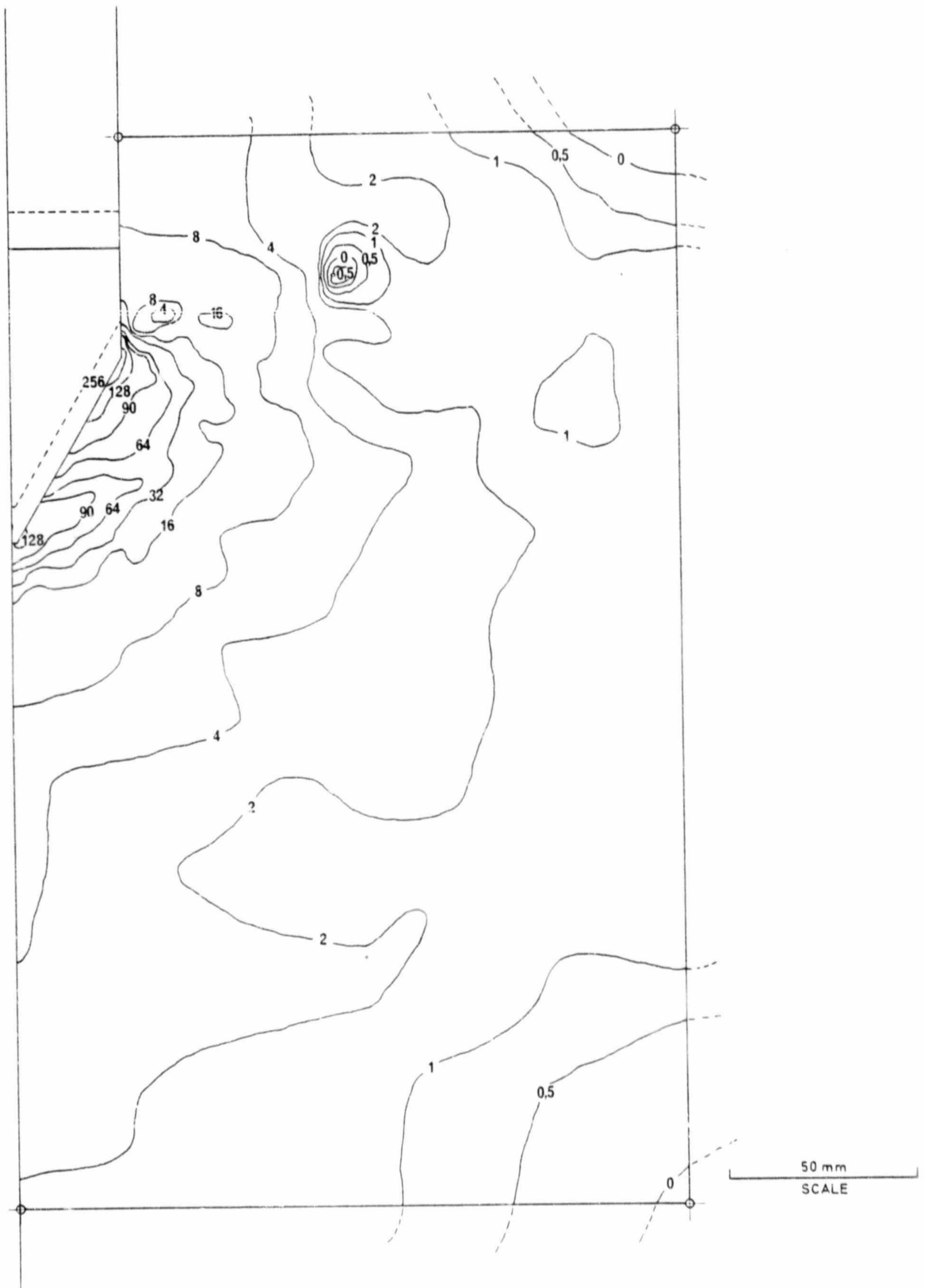

FIGURE 6.14 Major principal strain contours at $10^3\mu$-strain. Plates 1-3 Dynamic.

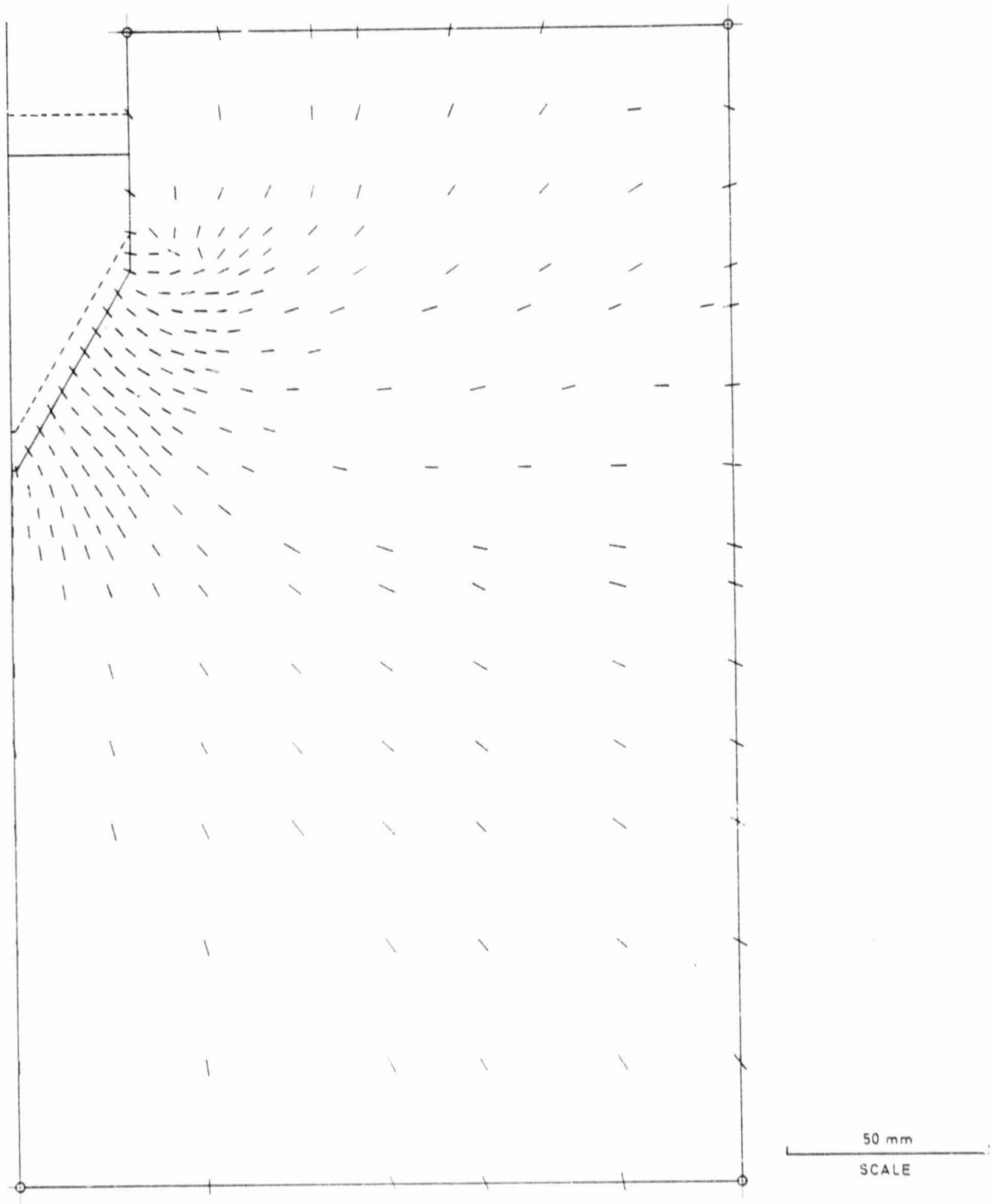

FIGURE 6.15 Major principal strain directions. Plates 1-3 Dynamic.

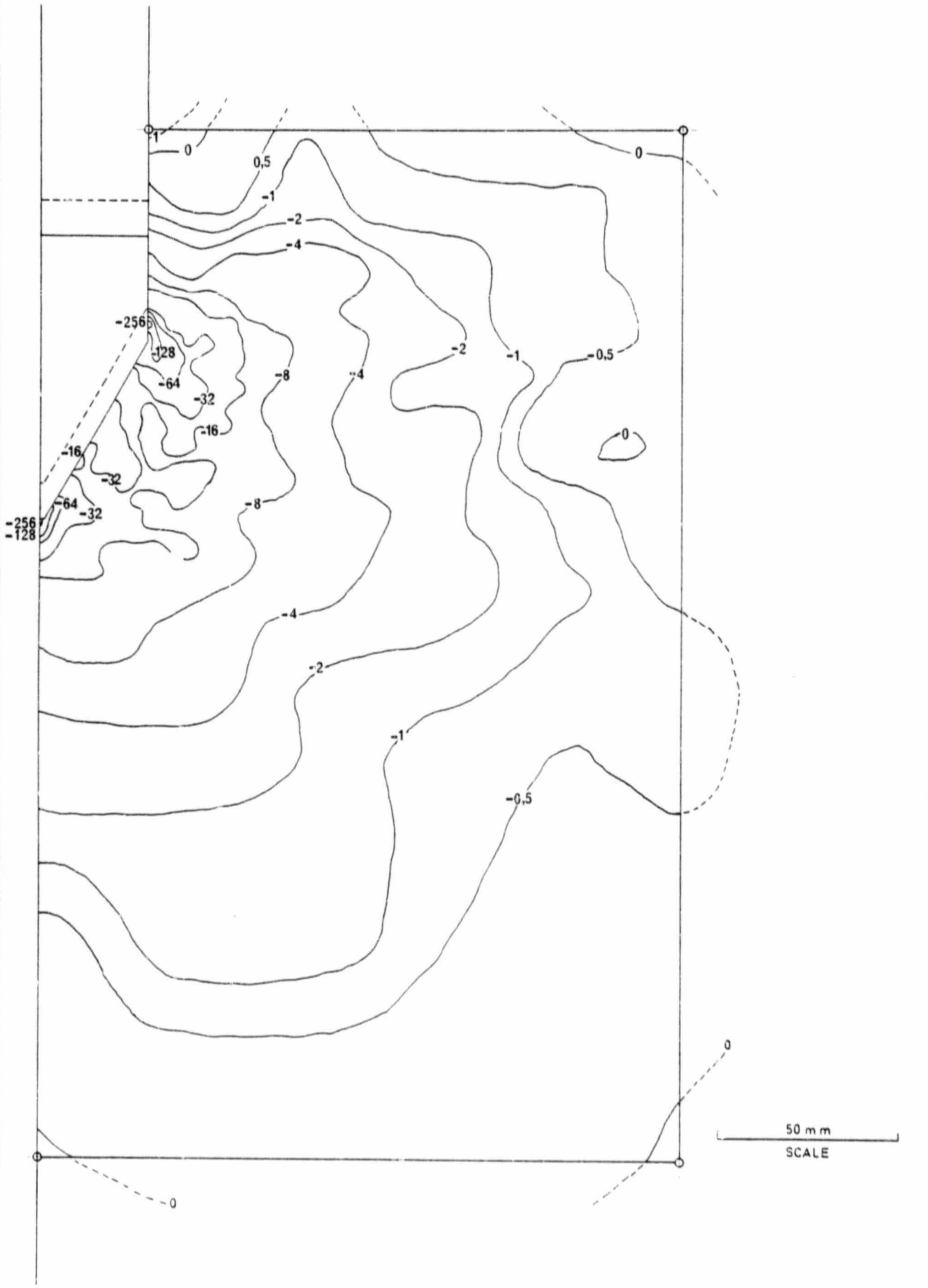

FIGURE 6.16 Minor principal strain contours at 10^3 μ-strain. Plates 1-3 Dynamic.

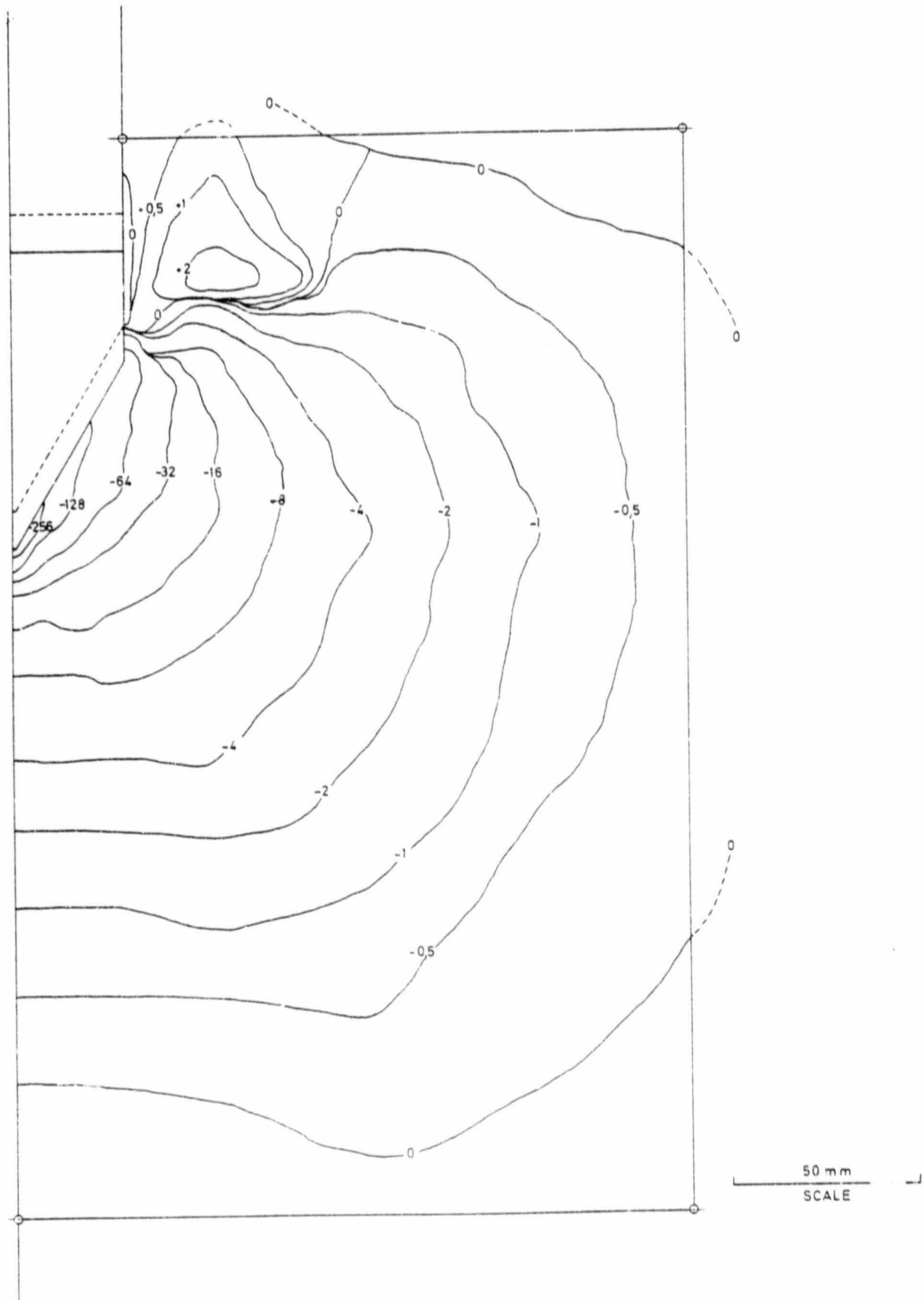

FIGURE 6.17 Circumferential strain contours at $10^3\mu$-strain. Plates 1-3 Dynamic.

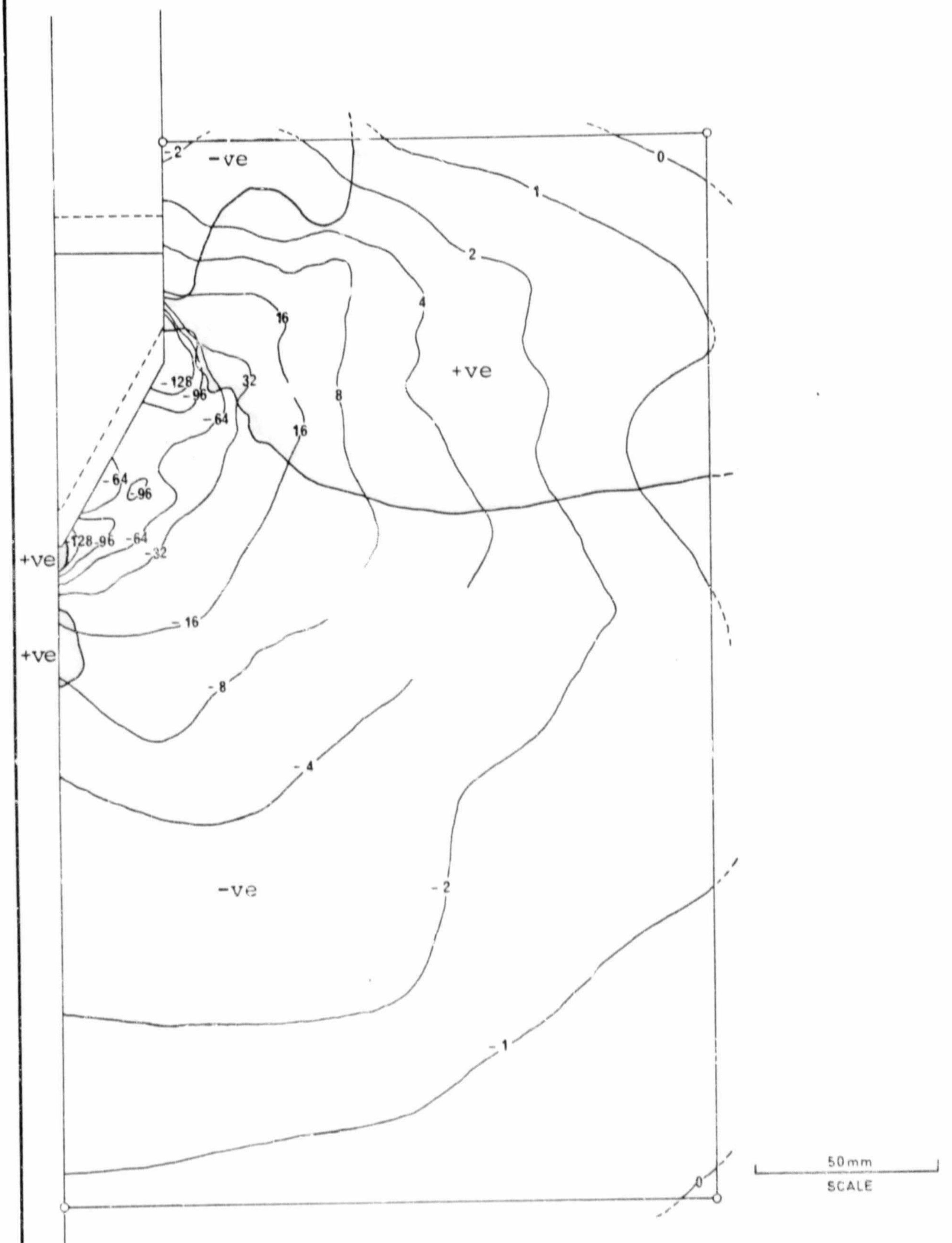

FIGURE 6.18 Maximum shear strain contours at $10^3\mu$-strain.
Plates 1-3 Dynamic.

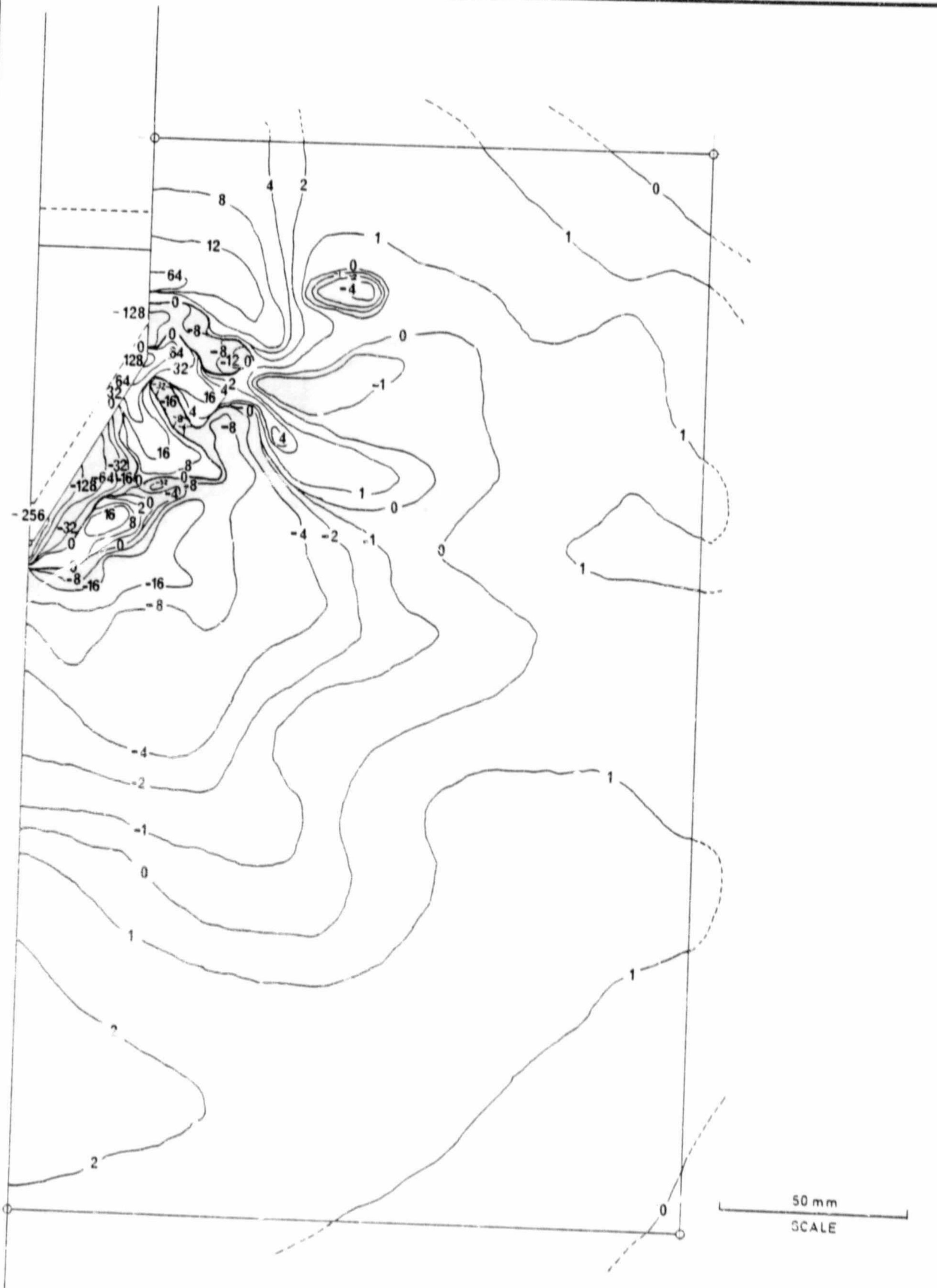

FIGURE 6.19 Volumetric strain contours at 10^3 µ-strain.Plates 1-3 Dynamic.